EXPLORATION OF THE CONTRIBUTION OF *PLASMODIUM* GRASP TO MULTIPLE PARASITIC STAGE DEVELOPMENT, WITH SPECIAL FOCUS ON METAMORPHOSIS IN THE LIVER

by
Ella Gehrke

A thesis submitted to Johns Hopkins University in conformity with the requirements for

the degree of Master of Science

Baltimore, Maryland
April 2020

Abstract

The *Plasmodium* parasite undergoes dramatic morphological and metabolic transformations as it adapts to diverse environments within a mosquito vector and a vertebrate host. During liver infection, the morphological changes of sporozoites (insect forms) includes the elimination of micronemes, organelles previously required for hepatocyte penetration. Preliminary experimental evidence suggests that *Plasmodium* utilizes an autophagic pathway that shares components with the unconventional protein secretion (UPS) pathway for microneme clearance from liver forms. The UPS pathway is implicated in the sequestration and expulsion of damaged proteins or organelles, bypassing the endoplasmic reticulum, instead requiring ATG8, and the Golgi reassembly and stacking protein (GRASP), a process called exophagy. In exophagy, GRASP has been identified as a molecular effector, tethering autophagic vesicles to the cell plasma membrane for cargo release. A GRASP ortholog is present in *Plasmodium* but its physiological role remains elusive. To investigate the relevance of *Plasmodium* GRASP to malaria infection, we have engineered a knockout *Plasmodium* mutant, named PbGRASP-KO (*Plasmodium berghei* GRASP Knockout). The objective of this study is to explore the role of *P. berghei* GRASP through all stages of the parasite's lifecycle, and particularly the possible involvement of GRASP in exophagy of micronemes during liver stage development. If PbGRASP-KO parasites are unable to clear micronemes during the transformation of sporozoites to liver stage trophozoites, this will subsequently impact parasite multiplication in the liver. Comparing the development of *P. berghei* WT and PbGRASP-KO in the mosquito, liver,

and blood stages, we show that PbGRASP-KO displays no growth defects in the mosquito and blood stages. However, after sporozoite inoculation of the PbGRASP-KO into mice, a spike in blood stage parasitemia was observed for several days. Interestingly, morphological examination of blood stage parasites after sporozoite inoculation shows a greater number of ring stage parasites than WT. Through fluorescence and electron microscopy of infected hepatocytes, we observe that the PbGRASP-KO was able to clear micronemes effectively, despite a more pronounced accumulation of micronemes beneath the parasite plasma membrane, and PbGRASP-KO underwent normal schizogony. We conclude that GRASP may have a role outside of the liver stage, perhaps during initial blood stage development.

Principal Investigator: Dr. Isabelle Coppens, PhD

Secondary reader: Dr. Photini Sinnis, MD

Contents

Table of Figures and Charts

Acknowledgements

I would not have been able to complete this master's thesis without the generous and kind help from the people in my life, to only a few I am able to give special thanks to here.

I would like to pay special regards to Dr. Isabelle Coppens for providing me a place amongst her team. It was a great privilege and honor to work in the Coppens lab under her leadership, where I learned the catalyst to scientific investigation is observation.

I would like to express my deepest and sincere gratitude to my research supervisor, Dr. Tejram Sahu, for providing invaluable guidance throughout my research. His passion for his work, creative mind, and patience for teaching provided the foundation for my thesis.

In addition, thank you to the rest of the Coppens lab team; Dr. Julia Romano, Dr. Karen Ehrenman, Beejan Asady, and Eric Hartman. Each of you dedicated time to help progress my work through your own experiences and wealth of knowledge. Additionally, you took time to engage me in hilarious and meaningful conversations that kept each day exciting.

Special thanks to Dr. Photini Sinnis for acting as my secondary reader. Your expertise and feedback helped bring this manuscript into success.

I would like to acknowledge and thank my parents, Jon and Laurie Gehrke, for your tremendous, unwavering support of my goals.

Lastly, I would like to thank my partner, Jack. Your love and friendship aided me more than you know.

List of Abbreviations

ACBP	Acyl-CoA binding protein
ACTs	Artemisinin combination therapies
ATG	Autophagy-Related Gene
ATG8-OE	Autophagy-related gene 8 over expressor mutant
bp	Base pair
CPS	Conventional protein secretion
CSP	Circumsporozoite protein
DAPI	4′,6-diamidino-2-phenylindole
DMEM	Dulbecco's Modified Eagle Medium
DMSO	Dimethyl sulfoxide
EEFs	Exoerythrocytic forms
EM	Electron microscopy
ER	Endoplasmic reticulum
FBS	Fetal bovine serum
FAC	Flow cytometry assay
gDNA	Genomic deoxyribonucleic acid
GRASP	Golgi reassembly and stacking protein
hDHFR	Human dihydrofolate reductase
h	Hours
hc	Host cell
IMC	Inner membrane complex

IFA	Immunofluorescence assay
MC	Maurer's clefts
αMEM	αMinimum essential medium
MSP1	Merozoite surface protein 1
MVB	Multivesicular bodies
PBS	Phosphate-Buffered Saline
PCR	Polymerase chain reaction
ph	Phagosome
p.i.	Post-infection
PS	Penicillin-Streptomycin
PV	Parasitophorous vacuole
qRT-PCR	Quantitative reverse transcription polymerase chain reaction
RBC	Red blood cell
RNA	Ribonucleic acid
RT-PCR	Reverse transcription polymerase chain reaction
TRAP	Thrombospondin-related anonymous protein
UPS	Unconventional protein secretion
UTR	Untranslated region
WT	Wild type

Introduction

Epidemiology and current options against malaria

Malaria is a globally prevalent, immensely debilitating disease. With half of the planet's population living in endemic countries, the public health significance of malaria cannot be understated (1). The causative agent, the apicomplexan *Plasmodium* spp., is transmitted through the bite of an infected elusive insect and is responsible for a reported 219 million malaria cases each year, and ~450,000 deaths (1). Although the morbidity and mortality of malaria are staggering, the case number has decreased from 239 million cases reported in 2010 (1). Progress is largely due to the immense effort by the global health community to reduce malaria mortality and morbidity through the improvement of vector control and the distribution of antimalarial drugs (1). With ~20 million fewer malaria cases in ten years, progress towards eliminating malaria is reasonably optimistic from a clinical and economic standpoint (1). However, it is important to recognize that previous progress in the reduction of malaria has stalled, with morbidity increasing by an estimated 2 million cases in 2018 compared to 2016 (1). In endemic countries, the burden of disease most heavily falls on pregnant women and children under the age of five, children under five represented 61% of all malaria deaths in 2017 (1). The increased risk of malaria infection in children is due to a loss of maternal antibodies and a lack of specific immunity to the *Plasmodium* antigens (2).

Antimalarial drugs have had a significant impact on the reduction of global malaria deaths. Artemisinin combination therapies (ACTs) are considered the gold standard of

antimalarial drugs due to drug potency, targeting all stages of the blood stage parasite (3). The WHO recommends ACTs as the first line treatment for all global malaria cases; however, *Plasmodium falciparum*, the species of *Plasmodium* causing greatest disease burden and mortality in humans, has historically been the primary target (3). The success of ACTs has led to broad use, and unfortunately, resistant populations of *P. falciparum* in South East Asia have already emerged (3, 4).

Vaccines are an ideal public health asset, as they strengthen the immune system to combat an infection prior to clinical manifestation of disease symptoms through the establishment of immune memory. Currently, the RTS, S /AS01 vaccine is the only licensed malaria vaccine for human use (5). RTS, S is a recombinant protein-based malaria vaccine that contains antigenic peptides derived from the circumsporozoite protein (CSP) of *P. falciparum*, mixed with a liposome adjuvant (6). Targeting CSP can block the sporozoite form of the parasite from invading a hepatocyte, preventing the progression of the parasite's lifecycle into the blood, and stopping clinical symptoms of malaria before their manifestation. However, the RTS, S/AS01 vaccination regimen has shown to not protect the entire at-risk age group, such as children 1 to 3 months, and the rate of vaccine efficacy diminishes over time (6). During a phase 3 trial throughout seven sub-Saharan African countries, vaccine efficacy wanes from 27 to 18.3% in children 6-12 weeks of age, over a 48-month period (6). Children ages 5-17 months see vaccine efficacy wane from 45.1 to 28.3% over a 48-month period (6).

Emerging resistance to ACTs and limited success observed in current vaccine trials jeopardizes progress towards reducing malaria mortality and highlights the importance for

continued research on the biology of *Plasmodium,* in hopes of finding new drug targets and protective antigens.

The biology of the malaria parasite

In addition to *P. falciparum*, human malaria is caused by four other *Plasmodium* species including *P. malariae, P. vivax, P. ovale, and P. knowelsi.* Illustrated in Figure 1, the *Plasmodium* life cycle begins when an infected female *Anopheles spp*. mosquito takes a blood meal, passing the infectious sporozoite from the salivary duct to a human host. The slender sporozoite is motile, and invasion-competent, possessing a cytoskeleton composed of microtubules, and an inner membrane complex (IMC), an organelle forming a double membrane layer beneath the parasite's plasma membrane, to maintain the pointed, elongated shape of the sporozoite until a hepatocyte can be located and penetrated (7, 8).

Once deposited in the host dermis, *Plasmodium* utilizes CSP that uniformly decorate the sporozoite surface for gliding motility, entering the bloodstream as the pathway to the liver (9). Once the sporozoite localizes to the host liver, CSP facilitates attachment to a hepatocyte, and the parasite can invade (9). The hepatocyte is an important cellular environment for the *Plasmodium* parasite, where it undergoes necessary replication prior to the clinically relevant blood-stage infection. Attachment and invasion are additionally facilitated through proteins discharged from microneme and rhoptry *Plasmodium* organelles in the sporozoite (10). Upon invasion, the parasite develops a parasitophorous vacuole (PV) derived initially from the cellular membrane of the host cell and then from material present in the rhoptry organelles (11). The PV is an important niche for the intracellular parasite, protecting it during replication through the evasion of host immune factors (12, 13). The unique membrane composition of the PV precludes fusion

with host destructive organelles such as lysosomes. The PV of *Plasmodium* liver forms is permeable to host cell solutes, allowing the *Plasmodium* parasite to acquire nutrients from its host (14). Following hepatocyte invasion, micronemes are expelled into the PV as they contain superfluous proteins that need to be purged from the sporozoite as it transforms into a replicative liver form (10). Inside the hepatocyte, the sporozoite begins to undergo dramatic morphological changes as it transitions from the slender infectious sporozoite to a round, metabolically active trophozoite, the first liver stage (7, 15). The cytoskeleton and IMC are dismantled and expelled into the PV space (16). Schizogony, a rapid replicative process of nuclear divisions, transforms the trophozoite into an exoerythrocytic schizont (17). As the parasite grows during the process of schizogony, it manipulates and stretches the hepatocyte, while generating new organelles for the developing asexually produced progeny (17). At the end of schizogony, merosomes packed with hepatic merozoites are surrounded by host plasma membrane and eventually burst the host hepatocyte (18). Merosomes, like individual coin purses filled with loose change, release thousands of mononucleated merozoites into the bloodstream of the host. Hepatic merozoites are invasion competent for red blood cells (RBC), transforming through erythrocytic forms of trophozoites and schizonts. The erythrocytic schizonts lyse host RBCs and release mononucleated erythrocytic merozoites into the blood, continuing the blood-stage cycle of *Plasmodium* (19). This cyclical pattern of invasion, replication, and egress in the blood stage is the pathological driver of the classical malaria disease symptoms (20). Antigens and parasite waste proteins released into the blood during RBC lysis induce cyclical bouts of fever and anemia (21). A subset of erythrocytic merozoites develops into a unique blood-stage form of sexual gametocytes, infectious to a female mosquito (21). When sexual

gametocytes are ingested by female mosquitoes during a blood meal, they mature into female and male gametes that fuse within the mosquito midgut, forming a fertilized zygote called an ookinete (22). The ookinete is motile and can traverse the mosquito midgut wall, developing into an oocyst (21, 22). Sporozoites form within the oocyst through asexual replication. After rupturing the oocyst, sporozoites migrate to the salivary glands of the mosquito host, where they wait for the mosquito's next blood meal to enter their next host to complete the cycle (21, 22).

Autophagy and *Plasmodium* metamorphosis

The *Plasmodium* life cycle involves multiple dramatic phenotypic transformations as it cycles through unique tissues of an insect and vertebrate host. For example, in a human host, *Plasmodium* must transform from the long and slender, invasion ready sporozoite to the rounded metabolically active, and replication-competent trophozoite in the hepatocyte (15). Organelles that are required for invasion and maintaining the sporozoite structure, such as the cytoskeleton, rhoptry, micronemes, and IMC, are no longer useful, and are eliminated from the parasite. During differentiation, many organisms discard organelles by autophagy (23, 24). Autophagy is a biological process utilized by eukaryotic cells to maintain homeostasis (23). This process can be utilized to eliminate redundant, senescent, damaged proteins or organelles, provide nutrients to the cell, or degrade intracellular pathogens, colloquially referred to as "housekeeping" activities (24).

In eukaryotic cells, conventional protein secretion (CPS) is considered the "standard" method for the trafficking of proteins. In the CPS pathway, cargo proteins are recognized through a transmembrane domain signal peptide and trafficked from the endoplasmic reticulum (ER) for protein folding and maturation, to the Golgi organelle,

where proteins are further processed and packaged into secretory vesicles (25). Processed proteins are then trafficked to a final destination (25). Unconventional protein secretion (UPS), less commonly described, is a pathway for the secretion of proteins lacking a signal peptide, thus bypassing the secretory pathway, and requiring autophagy machinery (25). In eukaryotic cells, the UPS is generally observed as a response to cellular stress, such as starvation or mechanical stressors (25). In the UPS, proteins are engulfed into an autophagosome that fuses with multivesicular bodies (MVB) to form amphisomes that then fuse with the plasma membrane to release the cargo. An UPS-like pathway can be also involved in the release of damaged proteins or organelles into the environment, named secretory autophagy or exophagy. In canonical (macro)autophagy, cargo is sequestered by a double sac membrane, that expands, developing into a closed autophagosome that fuse with lysosomes forming autolysosomes for degradation (26). Exophagy also involves the selective cytoplasmic enclosure of large cargo or organelles in autophagosomes, which fuse with MVB to form an amphisome, which can then be tethered to the cell plasma membrane, dumping cargo outside of the cell (10, 24, 25, 26, 27).

Autophagy Related Gene (ATG) proteins are responsible for the function and regulation of the UPS pathway (28). Through the sequencing of *Saccharomyces cerevisiae*, a yeast model with a characterized UPS pathway, and an in silico comparative analysis to the *P. falciparum* genome, ~15 orthologs of ATG proteins found in *S. cerevisiae* are also identified in *P. falciparum*. This indicates that the *Plasmodium* parasite has a rudimentary set of autophagy genes. Transcriptomic analysis suggests the autophagy orthologs found in *P. falciparum* have a role in induction and selection of cargo, the formation of a phagophore, assembly of the autophagosome from the phagophore, and degradation of the

autophagic body membrane (26, 29). Under drug stress, the formation of organellar structures in the cytoplasm that are analogous to autophagosomes, has been observed in the erythrocytic forms of *Plasmodium* prior to cell death, further confirming *Plasmodium* does possess and use the machinery for macroautophagy (30). Individual genes that consist of an ubiquitin-like ATG8 conjugation system facilitate the formation of the autophagosome and are all present in the *Plasmodium* genome (10). *Plasmodium* ATG8 proteins, structurally similar to ATG8 orthologs found in yeast, have been observed localizing to the apicoplast (an endosymbiotic plastid organelle), a potential spot for the derivation of proteins for the formation of the phagophore (15).

As previously mentioned, micronemes are eliminated from sporozoites during conversion into trophozoites (7). ATG8 structures have been observed colocalizing with micronemes identifiable by immunostaining of the microneme protein, thrombospondin-related anonymous protein (TRAP). In Figure 2, at 1-h post-invasion, TRAP is uniformly dispersed across a GFP-expressing *Plasmodium berghei* parasite. By 4-h post-infection (p.i.), the *P. berghei* parasite has begun to bulge in the center, the distal ends of the sporozoite pulling inward as it transforms into a rounded trophozoite. By 10-h p.i., the parasite has rounded fully, and the TRAP staining is found in distinct puncta as they are prepared to be expelled into the PV. At 24-h p.i., the *Plasmodium* TRAP are found within the PV, where they may be degraded (7). Importantly, lysosomal organelles have not been identified in the hepatic form of the *Plasmodium* parasite (10). The autophagosomes that contain micronemes to be eliminated, likely fuse with the parasite plasma membrane (10). Similar to the UPS for protein secretion, it remains possible that autophagosomes fuse with MVBs and the formed amphisomes fuse with the parasite plasma membrane in

Plasmodium liver forms for microneme evacuation, as depicted in the hypothetical model in Figure 3.

The importance of a secretory autophagy pathway to *Plasmodium* development is incentive for continued research into the biological pathways that mediate the transformation and survival of this complex parasite.

GRASP

In the mammalian cell, the Golgi complex plays a central role in secretion through the processing and packaging of macromolecules that, like proteins, are synthesized by the cell (31). With three functional distinct domains consisting of the cis, medial, and trans, the Golgi complex is engaged in the CPS pathway, which leads to the secretion of cellular cargo outside of the plasma membrane or the internal degradation of cargo through fusion with lysosomes (32, 33). Peripheral proteins called Golgi reassembly and stacking proteins (GRASP), are ubiquitous across all eukaryotic cells and engage the Golgi organelle at the surface membrane (33). Mammals possess two GRASP genes, referred to as GRASP55 and GRASP65 (32, 34, 35, 36). A conserved myristoylation motif is located at the N-terminus of GRASP55 and GRASP65 and has been identified as the binding motif that facilitates specific protein–protein interactions, and the association of GRASP proteins to cellular membranes (37). The tethering nature of GRASP is responsible for the formation of the stacked cisternae structure of the mammalian Golgi organelle, as depicted in Figure 4 (38, 35).

As a tethering protein, GRASP has also been characterized in the eukaryotic cell's UPS pathway during periods of cellular stress (32). Acyl-CoA binding protein (ACBP) has been studied as a model for the unconventional protein secretion pathway in *Dictyostelium*

discoideum (13, 39). ACBP secretion is necessary for the differentiation of spores but lacks a signal peptide, preventing engagement in the CPS pathway. Through gene deletion assays, ACBP secretion has shown to be entirely dependent on GRASP and autophagosome machinery, including ATG8/LC3, for autophagosome formation and amphisome secretion from the cell membrane (13, 39). GRASP is observed localizing to the cell plasma membrane, possibly facilitating the tethering of amphisomes to the cell plasma membrane (13). In mutant *D. discoideum* lines with the GRASP gene knocked out, amphisomes containing ACBP do not leave the cell membrane, and congregate near the cell membrane surface (13, 39).

UPS in eukaryotic cells could provide insight into GRASPs role in the *Plasmodium* secretory autophagy pathway. Unlike the related apicomplexan *Toxoplasma gondii*, which possesses a stacked Golgi organelle anterior to the nucleus of the parasite, *Plasmodium* parasites lack a defined stacked Golgi organelle (40). The *Plasmodium* Golgi organelle is dispersed through the cytosol of the parasite and is comprised of unstacked cis and trans-cisternae (41). The structure of the *Plasmodium* Golgi could suggest that GRASP does not have a role in the tethering of Golgi cisternae. However, *Plasmodium* does have an ortholog of a GRASP gene. Additionally, analysis of *P. falciparum* in the asexual blood stage shows PfGRASP also possesses an N-terminal myristoylation motif (42). Could this suggest that the function of the *Plasmodium* GRASP gene is specific to UPS? If so, GRASP could be of critical importance in *Plasmodium* autophagy for the elimination of micronemes, a process that has already been emphasized as highly important for parasite transformation and survival.

As shown in Figure 5, reverse transcriptase-polymerase chain reaction (RT-PCR) has detected the level of GRASP expression in the liver over time at 1, 2, and 3 days p.i., with *P. berghei* (10). PbGRASP is expressed throughout the liver stage development of the parasite, further supporting the hypothesis that there is a potential role for GRASP in the transformation that occurs from invasion to late liver stage.

Aim

The objective of this study is to explore the role of GRASP in *P. berghei* through all stages of the parasite's lifecycle and its possible involvement in exophagy during liver stage development.

Materials and Methods

Reagents and antibodies

All chemicals were obtained from Sigma (St. Louis, MO) or Thermo Fisher Scientific (Waltham, MA) unless otherwise stated. Antibodies used for the immunofluorescence assays included: Mouse anti-CSP (3D11) and mouse anti-HSP70 (4C9) (diluted at 1:100), a generous gift from Prof. Fidel Zavala (Johns Hopkins University) and rabbit anti-TRAP (diluted at 1:100) kindly provided by Prof. Photini Sinnis (Johns Hopkins University), and rat anti-ATG8 (diluted at 1:300) (7). All DAPI staining was performed at a dilution of 1:1000 with a concentration of 1 μg/ml. Secondary antibodies used for immunofluorescence assays included: anti-mouse (Alexa-488), anti-mouse (Alexa-555), anti-rabbit (Alexa-647), and anti-rat (Alexa-488).

Mammalian cell lines, bacterial cells and parasite strains

The commercial mammalian cell line used in this study is mouse Hepa1-6 (ATCC, CRL-1830). The transformed *E. coli* cells are One Shot® TOP10 Chemically Competent *E. coli* (Thermo Fisher, USA). The Hepa1-6 cell line was chosen for its monolayer growth pattern and grown in cell medium consisting of αMinimum essential medium (αMEM) with 10% Fetal Bovine Serum (FBS), 2 mM of L-Glutamine, 100 U/ml of Penicillin-Streptomycin, and 0.25 μg/ml Fungizone at 37°C in an atmosphere of 5% CO_2. One Shot® TOP10 Chemically Competent *E. coli* were grown, after transformation with appropriate plasmid, in LB medium containing 100 μg of ampicillin. *P. berghei*

ANKA was selected as the background strain for our study due to the use of the previously generated mutant ATG8 Over Expressor (PbATG8-OE). Generation of an ATG8-OE and PbGRASP-KO under the same strain can be used to generate information regarding the relationship between PbGRASP and ATG8 in the *Plasmodium* secretory autophagy pathway.

In vivo malaria model

All procedures were conducted under the following permits issued to the Johns Hopkins University School of Public Health Institutional Animal Care and Use Committee protocol #MO19H482. Swiss Webster female mice were the chosen rodent model for all experiments. A grouping of 5 mice for each infection type was maintained across all experiments. All mouse dissections were performed under anesthesia, mice receiving 200 µL of ketamine per mouse (ketamine 100 mg/ml, and prochlorperazine (Acepromazine) 10 mg/ml in 0.9% saline).

Plasmodium sporozoite cultivation

Salivary glands were dissected from infected female *Anopheles stephensi* mosquitoes between 21 and 26 days p.i. and stored on ice in 1X Phosphate Buffered Saline (PBS). A 27.5-gauge needle was used to disrupt the salivary glands and release *P. berghei* sporozoites, before dilution in 1X PBS for *in vivo* infection. For infection of Hepa1-6 cells, dissected salivary glands were stored in αMEM with 100 U/ml of Penicillin-Streptomycin (PS), and 0.25 µg/ml of Fungizone. Sporozoites were further diluted in 2% FBS in 1X PBS before counting using a C-Chip hemocytometer.

Cloning

To assess the role of PbGRASP in the development of the *Plasmodium* parasite, a GRASP knockout (PbGRASP-KO) mutant was generated by Dr. Tejram Sahu at Johns Hopkins University. The cloning plasmid, pDEF, a generous gift from Prof. Sean Prigge (Johns Hopkins University), was used as it has the selection marker, human dihydrofolate reductase (hDHFR), that helps with the selection of transformed clones.

A selection of a 1259 base pair (bp) region downstream of the PbGRASP gene and an 889 bp region upstream of the PbGRASP gene represent the respective 3' and 5' untranslated regions (UTRs) that flank our gene of interest. The UTRs were amplified from *P. berghei* genomic DNA (gDNA) using EXPAND ™ High Fidelity polymerase.

A forward and reverse primer (primers 1, 2) were designed to specifically amplify the 5' UTR from *P. berghei* gDNA. Forward and reverse primers for the 3'UTR were also designed (primers 3, 4) (Chart 1). Each primer sequence contains restriction enzyme cut sites used for future digestion steps. Each 50 µl reaction is a composition of two master mixes; mix 1: deoxynucleotide mix (10 mM), forward primer 300 nM, reverse primer 300 nM, template DNA 200 ng, sterile double distilled water up to a total volume of 25 µL; mix 2: Expand™ High Fidelity enzyme 0.75 µL, Expand™ High Fidelity Buffer (10x) with 15 mM $MgCl_2$, sterile double-distilled water to a total volume of 25 µL. Polymerase chain reaction (PCR) was performed under the following thermocycler conditions: initial denaturation of 94°C for 5 minutes, followed by 5 cycles of 94°C for 30 seconds, 60°C for 30 seconds, 72°C for 1.5 minutes, 35 cycles of 94°C for 30 seconds, 60°C for 30 seconds, and 72°C for 1.5 minutes with an additional 5 seconds/cycle extension time for each cycle. A final extension cycle of 72°C was performed for 7 minutes and samples were stored at

4°C. PCR products were analyzed for their size by electrophoresis on a 1% agarose gel stained with ethidium bromide and imaged using UV light.

The amplified 5' UTR gDNA and the pDEF vector DNA were digested with HindIII and PstI restriction enzymes, cutting at the specific cut sites amplified by primers 1 and 2 (Chart 1). The cloning vector and 5'UTR restriction digestion occurred under the following conditions: 37°C for 60 minutes followed by a heat inactivation step of 80°C for 20 minutes.

The ThermoFisher™ Rapid DNA Ligation Kit was used to ligate the digested 5'UTR into the digested vector, at a 1:3 molar ratio of vector DNA (ng) concentration to insert DNA (ng) concentration. Four microliters of Rapid DNA Ligation buffer, 1 μL of ligase, and sterile double distilled water to a total volume of 20 μL was added to the vector-insert ratio. The ligation reaction proceeded at 22°C for 30 minutes, remaining at 4°C until transformation.

To clone the 3' UTR into the pDEF vector, the amplified 3'UTR and pDEF vector, now containing the 5'UTR, were digested with EcoRI and KpnI restriction enzymes, cutting at the sites amplified by primers 3 and 4 (Chart 1). The pDEF vector and 3' insert was incubated in a thermocycler at 37°C for 60 minutes followed by a heat inactivation step of 65°C for 20 minutes. The same ligation protocol was followed for the ligation of the 3'UTR into the pDEF vector that was completed for cloning of the 5'UTR, accounting for changes in vector and insert DNA concentration.

Transformation

Ten microliters of the recombinant plasmid were added to One-Shot TOP10 *E. coli* cells and placed on ice for 30 minutes. The cells were subjected to heat-shock at 42°C for

30 seconds and placed in ice water for 5 minutes. Next, 250 μL of SOC outgrowth media was added to the cells and incubated for 1 hour at 37ºC with continuous shaking at 220 rpm. The transformed *E. coli* cells (~80 μl) were plated on LB. agarose plates with 100 μg of Ampicillin. Plates were incubated for 16 hours (h) at 37°C. Multiple colonies were screened by plasmid minipreps and restriction digestion using appropriate restriction enzymes. Restriction positive clones were sequenced to confirm presence of both the 5' and 3' UTRs. Successfully transformed *E. coli* clones were preserved with a 1:1 ratio of 40% glycerol and bacterial cell culture and stored at -80°C.

Transfection

To transfect *P. berghei* (ANKA), naïve mice were interperitoneally infected with blood stage WT *P. berghei* parasites. Parasite infected blood was extracted through a terminal cardiac puncture at ~4% parasitemia, and further cultured for 22-h at 5% CO_2 and 37°C in 1640 RPMI parasite culture media that consists of 6 mL of Fetal Bovine Serum (FBS) to 1 mL of blood, 750 μL of HEPES (4-(2-hydroxyethyl)-1-piperazineethanesulfonic acid), and 300 μL of Neomycin. Cultured parasites were verified, by Giemsa stain, for the presence of healthy schizonts. The linearized targeting plasmid, containing the 5' and 3' UTR flanked by hDHFR cassette, and the AMAXA reagent were mixed with the naïve parasites schizonts and subjected to electroporation as described (43). Electroporated parasites were immediately mixed with ice-cold 1X PBS and intravenously injected into naïve mice. The mice were treated with Pyrimethamine beginning one day after parasite injection, for nine days to select for the mutant PbGRASP-KO parasites.

PbGRASP-KO mutant parasites were isolated from the mice through cardiac puncture when the parasitemia reached 3-4%. Saponin (0.2%) was added to a sample of

the whole blood at a 1:2 ratio and placed on ice for 5 minutes. Samples were spun at 5,900x*g* for 5 minutes and the resulting pellet was washed three times with 1 mL of PBS. The pellet was resuspended in 200 μL of 1X PBS, gDNA was prepared from the saponin lysed blood sample using the QIAamp^{TM} DNA Blood Mini Kit. Genomic DNA preps were used as a template for PCR to confirm the presence and directionality of the newly inserted hDHFR cassette, and absence of the PbGRASP gene. Primers 5, 6, 7, 8 (Chart 1) were designed to overlap the regions between the hDHFR cassette and the 5' and 3' UTRs for confirmation. Primers 5 and 6 amplified a 1428 bp region overlapping the hDHFR cassette and 5'UTR. Primer 7 and 8 amplified a 1398 bp regions overlapping the hDHFR cassette and 3' UTR. Additionally, gDNA was sequenced and run through NCBI BLAST to confirm the absence of the GRASP gene.

Blood from one mouse that received transfected parasites was diluted and injected into 50 naïve mice at 0.5 parasites per mouse, to develop blood stage mutant clones. 16 mice became positively infected, confirmed through blood smear. PCR amplification of the region between primers 5 and 8 was completed for all newly infected mice. All 16 mice were positively infected with the PbGRASP-KO mutants. Three clones (Clones 4, 13, and 16) were selected for further characterization.

Phenotyping the mosquito stage

To assess whether the GRASP gene has an impact on the development of the parasite within the mosquito, female *An. stephensi* were infected with WT and PbGRASP-KO parasites through controlled blood feeding, depicted in Figure 10. On day 17 p.i., infected female mosquito midguts were dissected and stained with 0.1% mercurochrome. Oocysts were counted immediately following dissection using a light microscope equipped

with a 40x objective. On day 22 p.i., salivary glands were dissected as described earlier and sporozoite yields were quantified.

Gliding motility assay

To assess whether the deletion of GRASP has an impact on sporozoite motility, we looked at the trails of CSP left by gliding sporozoites on a LabTek 8 well chamber slide. Dissected sporozoites were placed in the well chamber in RPMI 1640 culture medium for 45 minutes in a 37°C incubator. The sporozoite trails were fixed with cold fixative solution (10X PBS supplemented with 10% formaldehyde, and 27% glutaraldehyde) and incubated at room temperature for 15 minutes. Wells were washed 3 times with 1X PBS and stained with a mouse anti-CSP (3D11) antibody and incubated at 4°C overnight. The secondary antibody, anti-Mouse IgG (Alexa-488), was applied the following day at a 1:1000 dilution. Gliding trials were visualized, and images acquired through an oil immersion 63x objective on a Zeiss fluorescence microscope and a Hamamatsu ORCA-R2 camera.

Phenotyping the liver stage

To characterize the phenotype of the liver stage, 10,000 GRASP-KO or WT sporozoites were injected intravenously into mice, outlined in Figure 10. The parasitemia was determined by counting infected RBC on blood smears taken every 24-h for 6 days p.i. starting from day 3 p.i. The parasites were quantified using a light microscope equipped with an oil immersion 100x objective. Morphology of the blood stage parasites was determined by quantifying the number of different erythrocytic stages such as rings, trophozoites, and schizonts at day 4 and 5 p.i.

Investigation of liver stages in vivo

To further elucidate the role of GRASP in the liver stage of the parasite, an in vivo model was developed. As depicted in Figure 11, WT and PbGRASP-KO sporozoites were injected into mice at a dilution of 10,000 sporozoites per mouse. At 24, 40, and 72-h p.i., 5 mice from each group were anesthetized and the whole liver was extracted. At 72-h p.i. liver was extracted after complete perfusion with 10 ml of 1X PBS. The liver samples were placed in 50 mL falcon tubes containing 12 mL of TRIzol as described (44). Using a Rotor-Stator Homogenizer, liver samples were homogenized for 1 minute and placed in -80°C overnight. The samples were thawed at room temperature and vortexed for 30 seconds to let the layers of tissue and supernatant separate. From the supernatant, 1 mL aliquots were transferred to 1.5 mL microcentrifuge tubes. Samples were centrifuged for 10 minutes at 12,000x*g*. Next, 500 µL of the resulting clear supernatant was transferred to a new 1.5 µL microcentrifuge tube and 500 µL of TRIzol was added to the sample and vortexed. Next, 200 µL of chloroform was added to the reaction and tubes were shaken by hand for 15 seconds and incubated at room temperature for 3 minutes. The samples were then placed on ice for an additional 3 minutes and centrifuged at 12,000x*g* for 15 minutes. The upper aqueous layer containing RNA was transferred to a new 1.5 mL microcentrifuge tube (~400 µL) and the same volume of 70% ethanol was transferred to the sample, mixing the sample through pipetting. Seven hundred microliters of the mixture were used for RNA isolation using Quiagen™ RNeasy mini kit following the manufacturer's instructions. RNA concentration was measured using a nanodrop and diluted to a 1µg/µL stock.

Complementary DNA (cDNA) was synthesized from the single stranded RNA precipitated from the liver tissues samples following the SuperScript First-Strand Synthesis

System protocol by Invitrogen as described (44). Samples were stored at -80°C until further use.

DNA standards were prepared by amplifying *P. berghei* gDNA with the Velocity DNA polymerase. The 18S gene was chosen to estimate parasite load and mouse β-actin was chosen to normalize the data. To 300 ng of template *P. berghei* gDNA, 10 μL of 5x Velocity buffer, 2 μL of primer dilution, 5 μL of 10 mM dNTPs, 1 μL of Velocity polymerase, 0.25 μL of dimethyl sulfoxide (DMSO), and nuclease free water up to total volume of 50 μL was added in a PCR tube for both β-actin and 18S samples. PCR was performed under the following conditions: initial denaturation of 98°C for 5 minutes, followed by 35 cycles of 98°C for 30 seconds, 50°C for 30 seconds, and 72°C for 30 seconds. A final extension cycle of 72°C was performed for 7 minutes and samples were preserved at 4°C. PCR product size was confirmed by running the products on a 1% agarose gel with a 100 bp ladder to confirm band sizes of 134 bp for 18S and 154 bp for β-Actin amplification. PCR products were cleaned using the Quiagen™ Column PCR Cleanup kit.

Concentration of the 18S and β-actin PCR products were diluted to 1ng/μL using nuclease free water. Serial dilutions of 10^8, 10^7, 10^6, 10^5, and 10^4 of template DNA copies in 2 μL were generated for the standard curve. 18S (Primers 9, 10) and β-actin primer (Primers 11, 12) dilutions were prepared at a 1:1:18 dilution of forward primer, reverse primer, and nuclease free water as described (44) (Chart 1). To create the master mix, 12.5 μL of 2xSYBR Green PCR Master mix, 1.6 μL of β-actin or 18S primer dilution, and 8.9 μL Nuclease-Free water is mixed for each individual well. 23 μL of master mix was added to each well in a 96 well plate, with 48 wells containing the β-actin primer master mix and

48 wells containing the 18S primer master mix. Standard curve DNA dilutions and the sample cDNA were added in triplicate to the respective wells in 2 µL volumes. For "no template added" wells, 2 µL of Nuclease-Free water was added. The plate was sealed with Microamp Optical Adhesive Film Cover and spun at 300x*g* for 2 minutes. The plate was placed in a thermal cycler and the following protocol was followed: 15 minutes at 95°C, 40 cycles with 95°C for 20 seconds, 60°C for 30 seconds, and 72°C for 50 seconds. Quantifications were normalized to the mouse β-actin gene to overcome variability in the concentration of 18S cDNA.

Investigation of liver stages in vitro

Characterized in Figure 12, 1 mL of Hepa1-6 cells were added to a 15 mL falcon tube with 5 mL of cell medium (αMEM with 10% Fetal Bovine Serum (FBS), 2 mM of L-Glutamine, 100 U/ml of Penicillin-Streptomycin, 0.25 µg/ml Fungizone). Cells were spun at 1500xrpm (Backman Coulter Allegra 6r centrifuge - GH-3.8 rotor) for 5 minutes. Medium was discarded by vacuum to wash away excess DMSO from prior cell preservation steps. To the remaining cell pellet, 1.5 mL of cell medium was added to resuspend cell pellet. The cell mixture was added to a T25 flask. Cells were grown to 80% confluency, with cell medium changes every 24-h. To seed cells for infection, the cells were rinsed with 10 mL of pre-warmed 1X PBS. Next, 1 mL of trypsin was added along the cell layer and vacuumed out. Another 3 mL of trypsin was added to the cell layer, and the plate was moved to 37°C for 3-5 minutes to allow the cells to dislodge from the flask. Next, 9 mL of cell medium was added to stop the trypsin digestion. Cells were then transferred to a 15 mL falcon tube and spun for 5 minutes at 2000 rpm (Backman Coulter Allegra 6r centrifuge - GH-3.8 rotor). Post spin, the supernatant was vacuumed out and the

cells were resuspended in 5 mL of cell medium. To quantify the cells, a 1:1 dilution of resuspended cells was added to Trypan blue. Three 24-well plates, each containing 3 wells for WT and 3 wells for the PbGRASP-KO infection, were fixed with glass coverslips. Each plate is specific for cell fixation at 24, 48, or 67-h p.i. Cells were diluted and 100,000 cells in one mL were added to each well . Cell culture medium was changed every 24-h.

Twenty thousand sporozoites in 500 µL of dissection media were added to each seeded well and spun at 2000 rpm (Backman Coulter Allegra 6r centrifuge - GH-3.8 rotor) for 5 minutes. The infection was prolonged for 3-h at 37°C and washed three times with 1X PBS subsidized with 100U/mL of PS, and 0.25 µg/mL of Fungizone. Following the wash, 1 mL of cell medium was added to each well, and plates were returned to the 37°C incubator. Cells were fixed at different time points for IFA. For plates fixed past 24-h, cell medium was changed every 24-h, subsidized with 0.12 µg/ml of Mycamine.

Immunofluorescence assays (IFA)

At 24, 48, and 67-h p.i., wells were washed with 500 µL of 1X PBS and fixed with 250 µL of fixative solution (5 mL water, 1 mL of 10X PBS, 4 mL 10% formaldehyde, 8 µL 27% glutaraldehyde) then incubated at room temperature for 15 minutes, wrapped in aluminum foil to minimize light exposure. Following incubation, cells were washed twice with 1X PBS. Fixed cells were then permeabilized with 0.3% Triton X-100 in 1X PBS and incubated at room temperature for 5-7 minutes. Cells were washed twice with 1X PBS and placed in a blocking solution; 300 µL of 3% BSA in 1X PBS per well, and incubated overnight at 4°C.

Detection was performed with mouse anti-HSP70 (4C9), rat anti-ATG8, and rabbit anti-TRAP in 3% BSA in 1X PBS. Following primary antibody incubation, wells were

washed three times with 1X PBS (5 minutes/wash) and secondary antibodies were added to 3% BSA in 1X PBS; anti-mouse (Alexa-555), anti-rabbit (Alexa-647), and anti-rat (Alexa-488) (diluted at 1:1000). Plates were wrapped in aluminum foil and incubated at room temperature for 45 minutes, followed by a wash step with 1X PBS (5 minutes/wash). DAPI stock was diluted to 1 μg/mL and added to wells at a 1:1000 dilution and incubated for 5 minutes, followed by three wash steps with 1X PBS. Coverslips were removed and rinsed in 1X PBS and water before mounting onto a slide with 3 μL of ProLong Diamond antifade mounting solution. Slides were stored at 4°C in the dark until imaging.

Infected cells were visualized with the Zeiss microscope equipped with an oil immersion 100x objective and a Hamamatsu ORCA-R2 camera. Optical Z-sections with a 0.2 μm spacing were captured using the Volocity software. Images were deconvolved using an iterative restoration algorithm. Contrast of individual images was adjusted using Volocity software. Using the Volocity software, deconvolved images showing HSP70 fluorescence were used to obtain data on the average volume and area of WT and PbGRASP-KO. Using Volocity Software, DAPI fluorescence overlapping with HSP70 fluorescence was used to obtain the mean fluorescence intensity of the parasite's nucleic acid content.

Phenotyping the blood stage

To determine whether the GRASP gene has a functional role in blood stage development of *Plasmodium,* 0.01% of PbGRASP-KO or WT *P. berghei* infected blood was injected intravenously into two sets of mice, as depicted in Figure 10. The parasitemia was monitored for five days. Parasitemia was determined by counting infected red blood cells on blood smears taken every 24-h for 5 days p.i. The parasites were observed and

quantified, after Giemsa staining of blood smears, using a light microscope equipped with an oil immersion 100x objective.

Electron microscopy (EM)

For transmission EM, sporozoites isolated from mosquito salivary glands were maintained in Dulbecco's Modified Eagle Medium (DMEM) and 10% FBS for 12-h at 37ºC. Blood collected from infected mice was washed 3x in 1X PBS, fixed in 2.5% glutaraldehyde (EM grade; Electron Microscopy Sciences, Hatfield, PA) in 0.1 mM sodium cacodylate buffer (pH 7.4) for 1 hour at room temperature, and processed as described (45) before examination with a Philips CM120 Electron Microscope (Eindhoven, the Netherlands) under 80 kV.

Results

As we hypothesized that GRASP might be playing an important role as a component of autophagic organelle clearance during liver-stage development of *Plasmodium*, deletion of the GRASP gene would have an observable impact on the metamorphosis of the *Plasmodium* parasite. However, our goal was to study the effect of the GRASP gene deletion, using *P. berghei* as a model parasite, through all stages of the parasite's life cycle in order to identify GRASP function.

1. Successful generation of a PbGRASP-KO strain

   Four sets of transfections of the PbGRASP-KO construct were completed (Figure 6), and transfected parasites were injected into 4 individual mice, the transfection process is illustrated in Figure 7. After 9 days of drug treatment, parasites were harvested and gDNA from a fraction of the parasite population was isolated for further verification. Successful integration of the deletion construct was verified by PCR with primer pairs 5/6 (for 5' UTR) and 7/8 (for 3' UTR). As shown in Figure 8, amplification of a 1428 bp fragment with primer pair 5/6 and a 1398 bp fragment with primer pair 7/8 suggests the successful integration of the deletion construct into the parasite genomic locus. Additional smaller bands in Figure 8 suggests a mixed parasite population that required further cloning into individual parasite clones. For cloning, we infected 50 mice with 0.5 parasite/mice from one of the 4 transformant infected mice. Of the 50 mice infected with 0.5 mutant parasites per mouse, 16 became infected. Initial confirmation of a positive infection

was completed with Giemsa stained blood smears. The generation of the PbGRASP-KO was further confirmed by PCR of the transfected parasites, using primer pair 5/8 to amplify the 3981 bp region overlapping the 5' UTR, hDHFR selection cassette, and the 3' UTR (Figure 6). Primer 5 and primer 8 were designed from upstream of the 5' UTR (Primer 5) and downstream of the 3' UTR (Primer 8). An amplification of 3981 bp not only confirms the integration of the plasmid but also its integration in the right locus. Figure 9 illustrates this verification with all 16 mice expressing a PCR band slightly below 4 kilobases (kb). This assay provided confirmation that our mice were infected with the mutant PbGRASP-KO, and the blood stage of the parasite could be isolated for future work.

2. <u>The PbGRASP-KO strain develops normally in mosquitoes</u>

To investigate whether the GRASP gene deletion affects the development of *P. berghei* in the mosquito or has an impact on the quality of the infection. We infected *An. stephensi* mosquitoes by feeding on WT and PbGRASP-KO infected mice. On day 17, we dissected the mosquito midguts of WT and PbGRASP-KO (clone 4) infected mosquitoes (n=30) to quantify oocysts, and we observed that the difference in the oocyst yield was not significant (Figure 13A). PbGRASP-KO oocysts developed similarly to WT, and the intensity of the infection was not statistically significant between the two groups. On day 23 p.i., we dissected the salivary glands (n=30) from the same infection groups and quantified the average yield of sporozoites per female mosquito. We observed that the salivary gland sporozoite load was similar in WT and PbGRASP-KO clones 4 and 16. The

difference in the average number of sporozoites per female (14, 375 WT; 20,125 clone 4; 19,100 clone 16) was not significant when using the Mann-Whitney U test to compare each clone to WT (Figure 13B).

3. CSP trail left behind by PbGRASP-KO suggest that sporozoites are motile

We next examined whether GRASP is involved in the parasite motility. Sporozoite motility requires CSP expression through the secretory pathway and exposure at the plasma membrane, therefore GRASP deletion could impact secretion of CSP to the sporozoite plasma membrane. An IFA was conducted to visualize the trails of CSP left by gliding motile sporozoites. We observed that both PbGRASP-KO and the WT strain left similar swirling, circular random trails of CSP, shown in Figure 14, indicating that the PbGRASP-KO strain remained motile in the sporozoite form, and CSP was secreted by both strains.

4. PbGRASP-KO sporozoite infection leads to enhanced blood stage infection at day 5 p.i.

To investigate whether GRASP plays a role in the development of *P. berghei* in the liver, we injected 10,000 WT or PbGRASP-KO sporozoites intravenously into naïve mice, and monitored the parasitemia and prepatent period, namely the emergence of the parasite in the blood, for 6 days p.i.. Illustrated in Figure 15, on day 3 p.i., we observed that both WT and PbGRASP-KO strains did emerge from the liver stage into the blood stage but with fewer PbGRASP-KO

parasites; however, this value was not statistically significant according to a Mann Whitney U test.

On day 4 p.i., the PbGRASP-KO infected mice experienced a spike in parasitemia that surpassed the WT infection. The PbGRASP-KO infected mice continued to have an enhanced parasitemia that continuing from day 4 to day 6 p.i. On days 5 and 6 p.i., the PbGRASP-KO parasitemia was significantly higher from the WT when using the Mann-Whitney U test. We have tested this assay with more than one clone of PbGRASP-KO and observed the same parasitemia growth pattern (clones 4 and 16).

To provide more clarity on a potential phenotype during the emergence period from the exoerythrocytic stage to the erythrocytic stage, we analyzed the morphology of the blood stage parasites on day 4 and 5 p.i. after a sporozoite infection. Analysis of PbGRASP-KO (clone 16) showed a statistically greater number of rings compared to WT at day 4 ($p=0.0317$) and 5 p.i. ($p=0.0312$) (Figure 16).

5. Quantification of the parasite burden in the liver at different time points post infection

To determine whether the phenotype we observed in the prepatent period after a sporozoite infection is the result of a slight delay in the release of majority of the hepatic merozoites and/or determine if more hepatic merozoites are being produced during late liver stage, we infected mice with 10,000 sporozoites and harvested liver from infected mice at 24, 40, and 72-h p.i.. We amplified parasite

18S cDNA by quantitative Real Time PCR (qRT-PCR) to estimate the liver parasite load and normalized it with host β-Actin. As we saw the difference in parasitemia on day 4 p.i. onwards after sporozoite injection, we expect at 24-h both WT and PbGRASP-KO to have similar parasite load. If there is a difference in schizogony, we will assume a measurable difference at the 40-h time point. Otherwise, if there is a subtle delay in release of most of the merozoites by PbGRASP-KO, we expect to see a significant difference between WT and PbGRASP-KO at 72-h p.i. Surprisingly, we observed no difference in the liver parasite load between PbGRASP-KO and WT parasites at any time points (Figure 17). This suggests there is no difference in schizogony in the liver stage. However, the subtle delay in merozoite or merosome release might need measurement of liver parasite burden at multiple time points between 55-h and 72-h as merozoites starts to come to blood around 55-h in WT parasite.

6. <u>WT and PbGRASP-KO mutant produces similar yield of the exoerythrocytic forms (EEFs)</u>

We next investigated if GRASP could contribute to invasion of sporozoites to hepatocytes and/or egress of merozoites from hepatocytes in vitro. The number of EEFs were calculated by IFA at 24, 48, and 67-h p.i. of Hepa1-6 cells, and 100 fields of WT and PbGRASP-KO infected cells were analyzed at each time point. At 24, 48, and 67-h p.i., no difference in the average number of EEFs between WT and PbGRASP-KO was observed according to the Mann-Whitney U test (Figure

18). This suggests no obvious defects in parasite invasion and egress in the absence of GRASP.

7. At 24-h p.i., PbGRASP-KO liver stage parasites are larger than WT

Next, by IFA we analyzed the average volume of the PbGRASP-KO EEFs as they grew from 24 to 67-h p.i. in vitro. We observed a statistically significant difference (Median volume of 215.2 μm^3 vs 191.2 μm^3; p=0.0225) in parasite volumetric area at 24-h p.i. but not significant at 48-h or 67-h when using the Mann-Whitney U test (Figure 19). This suggests the early transformation in PbGRASP-KO parasites might be rapid as compared to the WT.

8. The surface area of PbGRASP-KO parasites was not significantly different from WT parasites

To further investigate if the PbGRASP-KO affected growth, the surface area of processed images was obtained using HSP70 staining at 67-h p.i.. The difference in the area of PbGRASP-KO and WT was not significant when using the Mann-Whitney U test (Figure 20). This suggests both WT and PbGRASP-KO parasites are developing normally in vitro.

9. Karyokinesis is normal in PbGRASP-KO and WT schizonts in the liver

To examine if there was more hepatic merozoite formation in PbGRASP-KO, we quantified the total fluorescence intensity of DAPI, a measure of the nucleic acid content of the developing parasite, as the PbGRASP-KO developed in vitro at

48-h p.i. We observed that the total fluorescence intensity of the PbGRASP-KO nucleic matter was not statistically significant from WT when using the Mann-Whitney U test (Figure 21). This suggests that both WT and PbGRASP-KO parasite have similar number of nuclei at 67h schizont stage.

10. PbGRASP-KO parasites compartmentalize micronemes for elimination

We next hypothesized that GRASP could be involved in microneme clearance from converting sporozoites according to our model in Figure 3. Hepa1-6 cells were infected with WT and PbGRASP-KO parasites and fixed at 24, 48, and 67-h p.i. to examine the fate of micronemes using anti-TRAP antibodies. Depicted in Figure 22, at 24-h p.i., fluorescence imaging shows TRAP staining of distinct and well-defined puncta, close to the parasites' surface membrane. In the WT parasite, the TRAP staining was more dispersed throughout and did not appear to be forming clear well-defined puncta (n=35). By 48-h p.i., TRAP could still be seen distributed across the WT and PbGRASP-KO parasites, while some of the TRAP had begun to congregate near the surface of the parasite or in the PV space (Figure 23). Interestingly, the TRAP staining was observed outside of the PV in both WT and KO, a possible indication that TRAP staining illuminated PVM evaginations into the host cell cytosol. At 67-h p.i., TRAP has almost entirely been expelled into the PV of both WT and PbGRASP-KO strains (Figure 24). We also performed ATG8 staining using anti-ATG8 antibodies. ATG8 and TRAP signals were seen in partial colocalization from 24 to 67-h p.i., suggesting an elimination of micronemes through exophagy in both lines. Additionally, at 67-h p.i. ATG8 staining appears

to be in branched structure reminiscent of the apicoplast organelle, a possible site for the derivation of proteins for phagophore assembly (Figure 24). The IFA image data reveals that unexpectedly, GRASP does not play an essential role in the process of microneme clearance from liver forms.

We then performed EM observations on PbGRASP-KO sporozoites maintained under axenic conditions in culture medium for 12-h (7, 46). The process of conversion is initiated with the dismantling of the IMC that corsets the parasite and the IMC detachment from the parasite plasma membrane, which allows the parasite to expand in size and volume (Figure 25 – A, panel a). Micronemes are then sequestered in a double sac membrane in the parasite cytosol (Figure 25 –A panel b). We observed these same steps in KO parasites: the dissociation of the IMC from the parasite plasma membrane (Figure 25 – B, panels a-c), the compaction of the IMC in the cytoplasm (Figure 25 – B, panels d and e) followed by expulsion into the environment (Figure 25 – B, panel f) and sequestration of micronemes into a double membrane structures (Figure 25 – B, panel g). These observations further indicate that GRASP is not essential for any of the conversion steps, as PbGRASP-KO parasites convert normally into liver forms.

11. <u>The PbGRASP-KO strain has a normal replication rate in the blood</u>

Previous studies have analyzed the GRASP ortholog in *P. falciparum*. Using RT-PCR, PfGRASP expression was observed across the asexual blood stage (42). A study using PfGRASP antibody showed that GRASP remained within the parasite throughout the asexual period, and colocalized with the cis-Golgi marker

ERD2 (ER-retention-defective complementation group 2) (42). The expression of GRASP during the blood stage lead us to investigate whether the development of a blood stage infection would be dysregulated or impaired in a PbGRASP-KO strain compared to WT parasites. To assess the development of the KO in the blood, we injected equal numbers (0.01% final parasitemia) of erythrocytic forms of PbGRASP-KO or WT parasites into naïve mice and monitored the replication of PbGRASP-KO and WT parasite by measuring parasitemia for 5 days p.i. on blood smears. Detailed in Figure 26, the parasitemia of both groups developed equally overtime. This study was repeated for three PbGRASP-KO clones (clones 4, 13, and 16). The same growth pattern was observed for all clones which is similar to WT parasites. For blood stage comparison, One-way ANOVA/Kruskal-Wallis Test: $P>0.999$ was used. Each PbGRASP-KO clone was tested against WT with a Mann-Whitney U test. Finally, we inspected the morphology and organellar content of PbGRASP-KO in the blood stage by EM. Similar to WT parasites, the KO strain exhibited a normal ultrastructure, without cytopathies (Figure 27). Maurer's clefts, membranous tubular structures secreted by the parasite and dispersed in the host RBC cytoplasm, were also observed, indicating that GRASP seems not involved in the exportation of parasite material beyond the PV membrane.

Discussion

As it cycles between hosts, *Plasmodium* must adapt to new environments within the definitive mosquito host and a vertebrate host. The adaptation to these environments is mediated by dramatic transformations reliant on autophagy, to adjust parasite morphology and metabolism (10). The secretory autophagy pathway for organelle remodeling is critically important for the metamorphosis and development of *Plasmodium* parasites in the liver.

We hypothesize that an unconventional organelle expulsion pathway may be utilized in sporozoites during conversion into replicative liver forms. We previously illustrated that this process involves *Plasmodium* ATG ubiquitous genes that help in the formation of ATG8- associated autophagosome structures that engulf organelles to be discarded (10). To provide additional information on this pathway and identify other molecular effectors, we have investigated the role of *Plasmodium* GRASP, a major player in the UPS pathway in many organisms (13, 39).

We hypothesize that GRASP could function in the secretory autophagy pathway of *Plasmodium* during morphological transformations between hosts and tissues. We have explored the *P. berghei* GRASP function by selectively deleting the *GRASP* gene (PbGRASP-KO) and phenotyping a PbGRASP-KO mutant through all stages of the parasite's life cycle.

The first stage we investigated was the development of the PbGRASP-KO strain in the mosquito host. To investigate whether the PbGRASP gene has a potential impact on the growth of *Plasmodium* within the midgut epithelium of a female mosquito, or can

impact the quality of the mosquito infection, the PbGRASP-KO parasites were monitored through the mosquito host for 21 days p.i. Quantification of the PbGRASP-KO oocysts on day 17 and sporozoite forms on day 21, together they indicate that there is no difference in the average oocyst or sporozoite numbers compared to the WT strain (Figure 13). The similarity in average yields suggests that PbGRASP does not have a significant impact on gametocyte fusion in the midgut, ookinete motility into the mosquito midgut epithelium, development of oocysts, asexual replication of sporozoites, or sporozoite motility and invasion of the salivary glands.

Additionally, we wanted to determine whether PbGRASP could impact the motility of the salivary gland sporozoite. Gliding motility is a characteristic that is essential in hepatocyte invasion by the sporozoite. Evaluation of CSP trails left behind by a motile sporozoite suggests that the PbGRASP-KO strain remains motile. Furthermore, the liver stage burden at 24 and 40-h p.i. by qRT-PCR, as well as the IFA images at 24-h p.i., suggest the PbGRASP-KO strain has no defect in motility, as it is equally infectious as WT (Figures 17, 24). This suggests that CSP secretion is not reliant on GRASP, GRASP does not participate in sporozoite motility during tissue traversal to reach the host liver, nor does the absence of GRASP result in a defect in motility.

Of primary interest was the role of PbGRASP in the liver stage. Previous studies show that the PbGRASP gene is expressed throughout the liver stage of the parasite (3 days p.i.) indicating a potential role for GRASP during this period of metamorphosis (10). The transformation from the invasion-competent sporozoite to a metabolically active trophozoite and schizont within a hepatocyte requires the parasite to transition from an arthropod to vertebrate cellular environment. To achieve this transformation, *Plasmodium*

expels superfluous micronemes that are no longer required for parasite survival after invasion of the hepatocyte (7). If the GRASP gene is expressed and has a role in the exophagy pathway during liver stage development, the PbGRASP-KO strain may not emerge into the blood at all or may be defective or delayed in blood stage infection.

Further examination of *Plasmodium* liver stage development is critically important, as it precedes the clinically relevant blood stage. The transfer of a sporozoite through the bite of a mosquito presents a bottleneck event for *Plasmodium*, as few sporozoites enter the bite site, a reported a mean of 123 sporozoites per bite, and a geometric mean of 36 sporozoites per bite (47). This bottleneck suggests that the asexual schizogony period within a hepatocyte is important for increasing parasite numbers and establishing infection within the vertebrate host. We hypothesize that for the liver stage, a phenotypic difference may appear when comparing the PbGRASP-KO strain to WT.

Evaluation of time to blood stage infection after injection of mice with WT or PbGRASP-KO sporozoites reveal that both strains began to emerge into the blood on day 3 p.i. This suggests the time required to blood stage infectious forms is similar in both WT as well as PbGRASP-KO parasites (Figure 15). However, the parasitemia started to diverge, the PbGRASP-KO strain having more parasitized RBC than WT from day 4 p.i.. From this point on, PbGRASP-KO infected mice had significantly higher parasitemia and remained high until day 6 p.i. (the last day of blood smear collection) (Figure 15). This was interesting, because when we later studied the effect of PbGRASP-KO on blood stage development, we found the pattern and rate similar to WT (Figure 26). This suggests that the phenotype is either derived from the liver stage or early blood stage.

One possible explanation is that while both strains lead to blood stage infection on the same day, some portion of the PbGRASP-KO liver stage parasites egress into the blood in a delayed manner, leading to a high blood stage infection starting on day 4 p.i. (Figure 15), which is supported partly by the statistically higher percentage of ring stage parasites in PbGRASP-KO than WT at day 4 and 5 p.i. (Figure 16). However, this is not supported by the quantification of parasite gene expression in the liver using qRT-PCR at 72-h p.i. This discrepancy might be due to the low initial parasite number or the time point selected for liver load estimation. We need to have multiple time points between 55h and 72h to effectively pin-point the difference in merozoite release. Additionally, the 18S gene selection could be replaced with the merozoite surface protein gene (MSP1). MSP1 can provide a more accurate parasite expression in the 40-72-h window, as at this stage Plasmodium has already differentiated to merozoite forms, which will allow us to better interrogate the late liver stage load. Additionally, a bioluminescent PbGRASP-KO would be helpful in continuous measurement of parasite liver load in real time.

To continue characterization of the observed liver stage phenotype, an in vitro liver stage culture was developed to observe the development of the exoerythrocytic forms over time by fluorescence microscopy. We showed that the PbGRASP-KO strain develops normally, with no observed major growth defect. However, up to 24-h p.i., PbGRASP-KO strain has a significantly larger volumetric area, without any increase in nuclear profiles (Figures 24, 25, 26, 27). Together this data suggests that there is not enhanced hepatic merozoite production in the PbGRASP-KO strain, which is in line with our in vivo assay results, indicating that the root of the enhanced blood stage infection may lie outside of the liver stage altogether. However, to further confirm that there is no increase in the number

of nuclei, an assay to amplify parasite nucleic acid through qRT-PCR would be more informative. Furthermore, evaluation of the development of hepatic merozoites in the first round of replication in RBC would be of interest to understand the difference observed between PbGRASP-KO and WT parasitemia after sporozoite injection. We hypothesize the role of hepatic merozoites in enhanced parasitemia in PbGRASP-KO because they are transcriptionally significantly different than blood stage merozoites and might result in a differential first cycle of parasite replication (48).

Of primary interest was observing whether PbGRASP is playing a role in the secretory autophagy pathway through the interaction with ATG8, to expel micronemes. Interestingly, the PbGRASP-KO strain appears to have more distinct, clear puncta of TRAP at 24-h p.i. This is suggestive that, at 24-h p.i., the PbGRASP-KO strain has better microneme compartmentalization than WT (GRASP-independent process), and the puncta are accumulated close to the parasite membrane surface, with a delay in microneme expulsion (possible GRASP-dependent process). One hypothesis for the PbGRASP-KO strain containing clearer puncta at 24-h could be that GRASP deletion results in an inability or stall in the tethering of amphisome structures to the parasite plasma membrane, resulting in a congregation of these vesicles near the surface. This hypothesis would be in line with what has been observed in *D. discoideum* (13, 39). Alternatively, GRASP, if involved in exophagy of micronemes, may act as a regulator, and in its absence in the KO, the sequestration of micronemes into autophagosomes and the delivery of autophagosomes to the plasma membrane could occur faster than in WT parasites. At 48 and 67-h p.i., we identified no other observable phenotypic difference when comparing the TRAP staining of PbGRASP-KO to WT during the in vitro infection. Successful clearance of micronemes

was observed in both the PbGRASP-KO and WT strain, indicating that GRASP does not have an essential role in microneme clearance as suspected initially. We also show that the PbGRASP-KO strain develops normally, with no observable growth defect (Figures 20, 21, 22). No ultrastructural defect was seen in the in vitro conversion of PbGRASP-KO sporozoites to trophozoites, the IMC and micronemes could be further observed during expulsion into the PV (Figure 25).

Previous studies observing autophagy of *P. falciparum* in the blood identified that ATG8, an autophagosome marker and ubiquitous protein in the autophagy pathway, associated with autophagosome-like vesicles during periods of blood stage starvation or drug stress (49). This suggests that the formation of autophagosome-like structures for conventional autophagy or secretory autophagy (exophagy), occurs in the blood stage of the parasite. Additionally, GRASP expression is present across the asexual blood stage of *P. falciparum* (42). If GRASP proteins participate in a secretory autophagy pathway, it is therefore plausible that in the absence of GRASP, this pathway could be dysregulated, and the *Plasmodium* infection cycle impaired, as the parasite is undergoing morphological transformations from merozoite to erythrocytic schizont forms between RBC infection, replication, and egress.

By infecting erythrocytic forms of the PbGRASP-KO and WT strains into mice, we observed that the PbGRASP-KO strain is able to develop identically to the WT strain in the blood, with similar parasitemia levels at days 2, 3, 4, and 5 p.i. as the WT (Figure 26). This study suggests that the deletion of the *Plasmodium* GRASP gene does not affect the growth and development of an established blood stage, nor does it affect the

maintenance of a blood stage infection over time. No ultrastructural defect could be observed in the KO blood stage parasites (Figure 27).

At this time, we have eliminated several points in the *Plasmodium* life cycle as potential areas where the GRASP gene may have an impact on the parasite development. The only phenotype we observed is the PbGRASP-KO strain parasitemia spike beginning on 4 days p.i. of a sporozoite infection. This assay has been repeated three times with separate clones, all producing the same results. We have not identified the reason for the enhanced blood stage infection induced by a sporozoite infection; however, we have further hypotheses that will guide future research.

It is possible that the higher blood stage parasitemia phenotype in the KO is due to enhanced replication of hepatic merozoites during the first round of schizogony in RBC after invasion of a hepatic merozoite. This could be possible if GRASP acts as a regulator to erythrocyte stage schizogony. The normal egression of the PbGRASP-KO into the blood, followed by the spike in parasitemia from day 4 to 6 p.i., could be explained by this enhanced replicative step. In order to further investigate this phenomenon, we could perform cardiac puncture of infected mice with the WT and KO strains 55-h p.i., followed by culturing of infected RBC, bringing the first round of erythrocytic blood stages to schizonts, and enumerate mononucleated merozoites per schizonts through microscopy and flow cytometry assays (FAC). This assay would be possible because rodent parasites do not reinvade fresh RBC during in vitro culture conditions and remain stuck in the schizont stage. This will allow us to determine if the first round of erythrocytic production of merozoites is dysregulated or enhanced. Additionally, evaluation of the merosomes, a life

stage we have not yet characterized for our PbGRASP-KO strain, to observe size, number, and egress would possibly shed light on the observed phenotypic difference.

Additional future plans include the development of an anti-GRASP antibody for the *P. berghei* ANKA strain. This will allow us to analyze the distribution of GRASP in all parasite stages, observe potential alterations in the Golgi morphology and assess whether the GRASP signal is associating with autophagy proteins, ATG8, and microneme proteins through colocalization, thus inform if GRASP intersect with the secretory autophagy machinery on liver forms.

To repeat the assays we have completed thus far, a new host model should be chosen. Pb-ANKA has differential RBC preference depending on the host. In general, the ANKA strain has a preference for the invasion of reticulocytes. However, in the mouse model we used, Swiss Webster, few reticulocytes are present, and the strain defaults to the invasion of normocytes. This is significant because the cell types the parasite invades will dictate the number of merozoites per schizont. With this in mind, we will need to repeat our experiments with Wistar rats, a host model that will allow our strain to mostly infect reticulocytes, removing the possibility that our assay is skewed by the differences in parasitized cell types.

Future research of the *P. berghei* GRASP gene would also benefit through exploitation of a luciferase expressing PbGRASP-KO mutant to observe the liver stage infection in live animals. Additionally, we hope to use flow cytometry to measure parasitemia in the blood of sporozoite inoculated mice, as it can more accurately detect low parasitemia. Both assays would allow us to better follow the PbGRASP-KO emergence from liver to blood in vivo and in vitro infections, so as to identify if a subtle merozoite

emergence delay does occur in the KO strain, which would be challenging to quantify through qRT-PCR.

Figure Legend

Figure 1

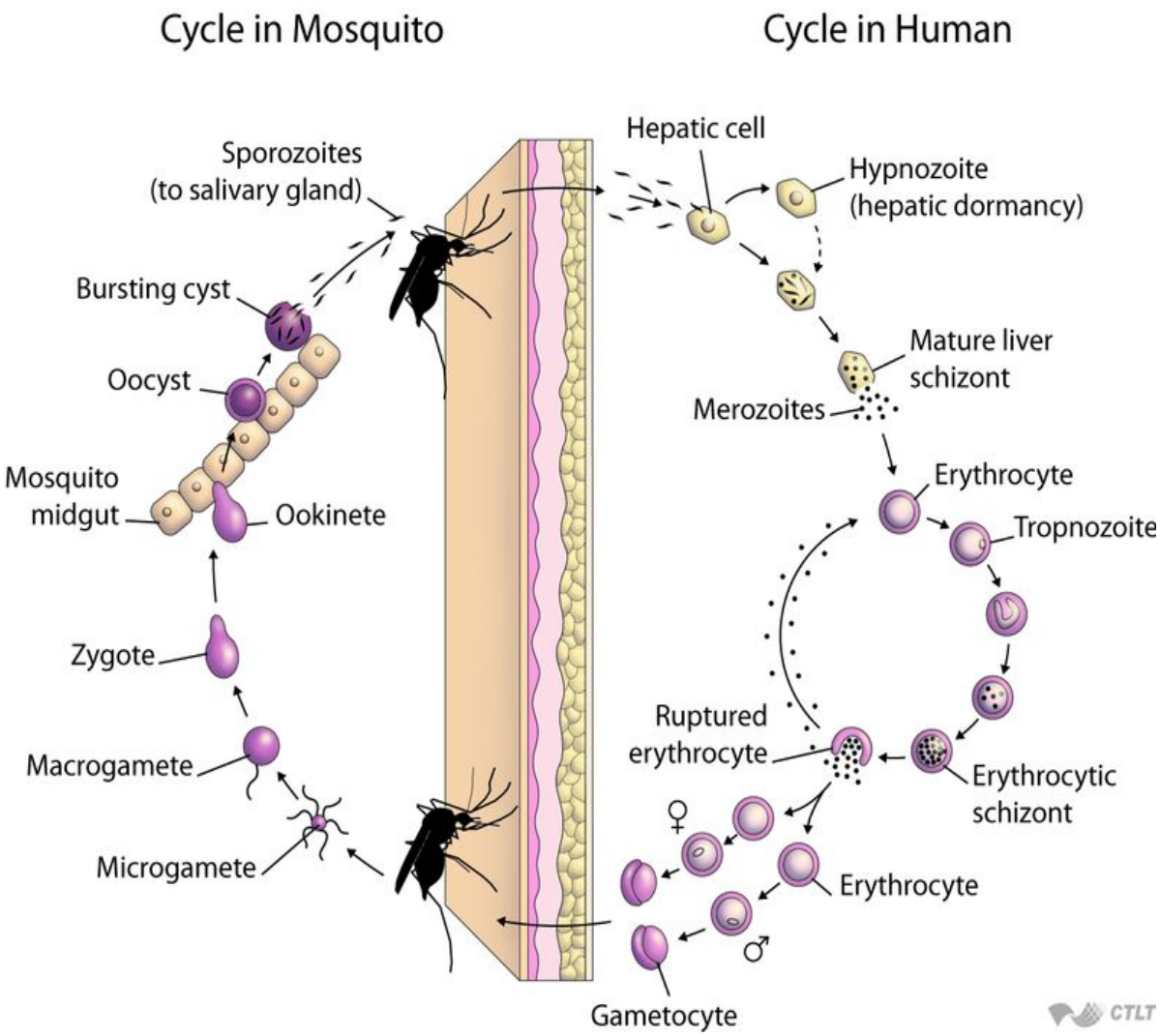

Figure 1 The *Plasmodium* Life Cycle

The *Plasmodium* parasite cycles between a definite female mosquito host and a vertebrate intermediate host.

Mosquito host: During a blood meal, the female mosquito ingests gametocytes, the sexual stage of the *Plasmodium* parasite. The gametocytes release gametes. Male and female gametes fuse in the midgut of the mosquito forming a zygote, which metamorphosed to a motile ookinete. The ookinete is motile and traverses the midgut epithelium. On the basal surface of the midgut epithelium, the ookinete transforms into an oocyst. Asexual reproduction within the oocyst generates the sporozoite stage of the parasite. Sporozoites burst from the oocyst and travel forward to the salivary glands of the mosquito, penetrating and invading the salivary gland tissues. Once in the salivary gland, the sporozoites undergoes final developmental changes and waits for the mosquito to take a blood meal.

Vertebrate host: During a mosquito blood meal, the sporozoite enters the host dermis, and migrates to the blood. The slender sporozoite now is carried to the host hepatocyte, where it can invade and undergo necessary replicative steps. The sporozoite transforms into a metabolically active trophozoite. Through the process of schizogony the trophozoite transforms into a hepatic schizont. When schizogony is completed, the schizont bursts from the hepatocyte, releasing merosomes packed with mononucleated merozoites into the blood. Hepatic merozoites invade RBCs, transforming through erythrocytic trophozoite and schizont forms. Schizonts lyse the RBC's and the infection continues with erythrocytic merozoites invading new RBCs. Some of the blood stage parasites differentiate into gametocytes that will be taken up by a mosquito to continue the transmission cycle.

Figure 2

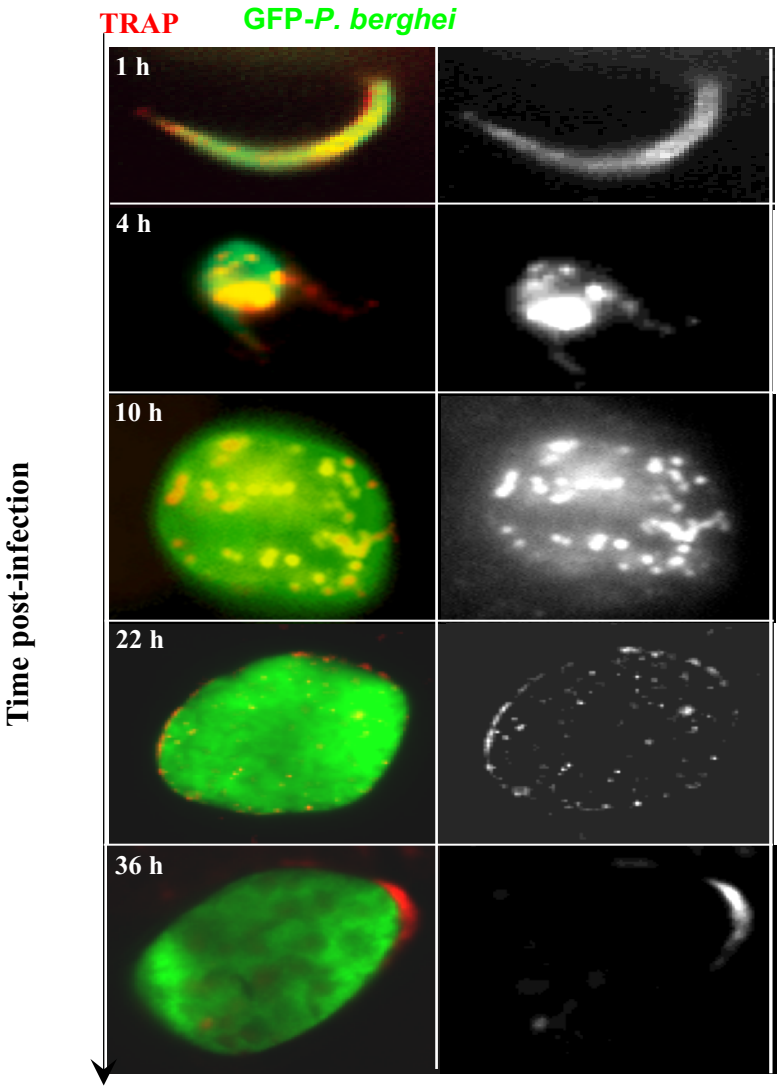

Figure 2 - Clearance of TRAP-containing micronemes from transforming sporozoite
A GFP-expressing *P. berghei* parasite within a Hepa1-6 cell is observed by fluorescence microscopy. Following invasion of the hepatocyte, the sporozoite begins to undergo dramatic morphological transformations from a slender and invasion competent sporozoite to a round, metabolically active trophozoite. At 1-h the TRAP signal with an anti-TRAP antibody (red) looks diffuse due to the small size of micronemes (25 nm diameter) that are dispersed throughout the cytoplasm of sporozoites, By 4-h p.i., the sporozoite begin to round in the center, drawing the distal ends of the pointed sporozoite inward. TRAP is still uniformly dispersed across the parasite surface at this time. At 10-h p.i., the TRAP begins to compartmentalize into distinct puncta, reflective of micronemes sequestered into autophagosomes. At 22-h p.i., the TRAP signal begun to be in the parasitophorous vacuole (PV). By 36-h p.i., the microneme TRAP has been almost entirely eliminated from transforming hepatic form of *Plasmodium* into the PV [adapted from 6].

Figure 3

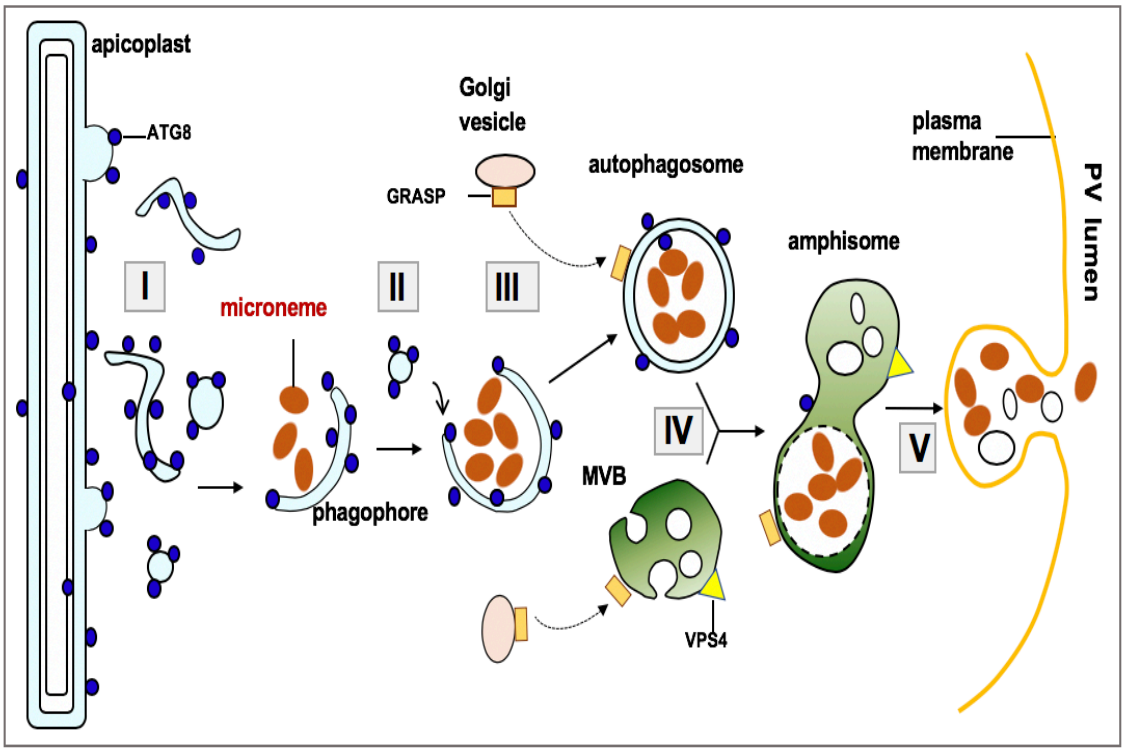

Figure 3 – A hypothetical model of the *P. berghei* Secretory Autophagy Pathway
I. ATG8-containing vesicles or tubules bud off from the apicoplast organelle.
II. ATG8 form cup-shaped phagophore that surrounds cytoplasmic contents, such as micronemes.
III. The phagophore continues to expand, forming an autophagosome vesicle, isolating micronemes
IV. GRASP proteins tether multivesicular bodies (MVB) and autophagosomes together, fusion induces the formation of an amphisome
V. GRASP tethers amphisome to plasma membrane, dumping microneme protein cargo into the PV lumen

.

Figure 4

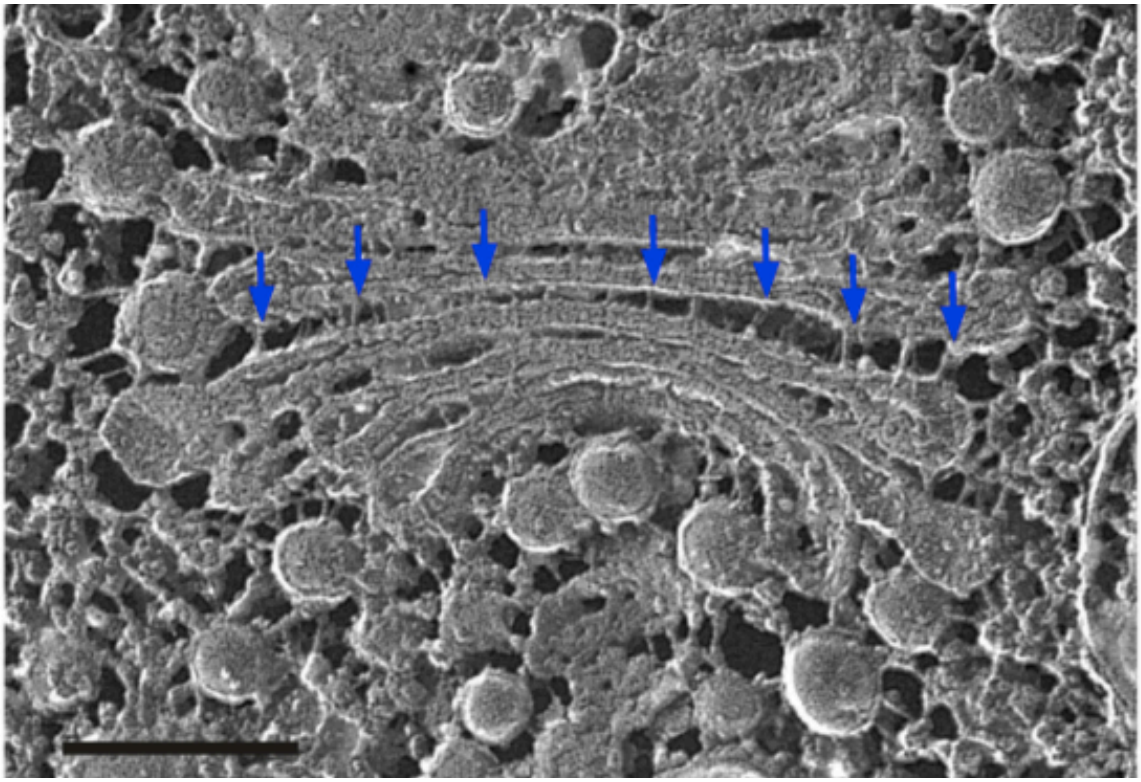

Figure 4 - GRASP establish the stacked cisternae structure of the mammalian Golgi complex
Myristoylation of the N-terminus on mammalian Golgi Reassembly and Stacking Proteins, GRASP55 and GRASP65 facilitate the tethering of Golgi cisternae into the stacked cisternae Golgi complex. Arrows in blue pinpoint the location of the GRASP proteins within the mammalian Golgi organelle [adapted from 50].

Figure 5

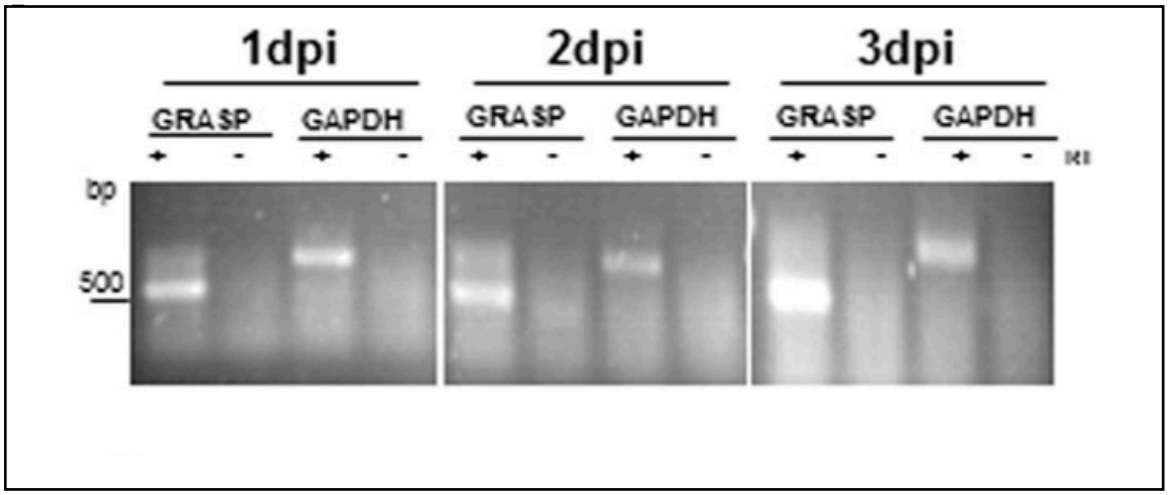

Figure 5 - Expression of *P. berghei* GRASP at 1, 2, and 3 days p.i. in the liver forms
Expression of PbGRASP in liver stage was measured in duplicate by RT-PCR over 1, 2, and 3 days p.i. GAPDH expression was used as an internal control. GRASP and GAPDH were both expressed on 1, 2, and 3 days p.i. [adapted from 10].

Figure 6

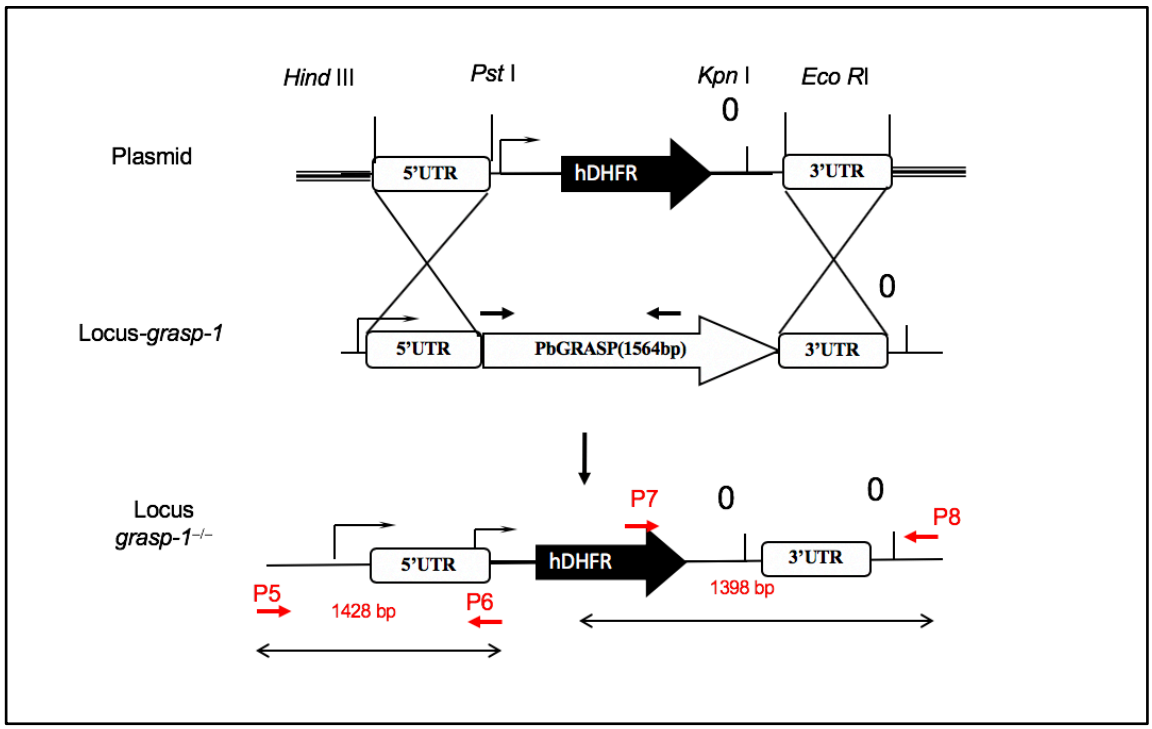

Dr. Tejram Sahu - Unpublished

Figure 6 - Homologous recombination strategy for the generation of the PbGRASP-KO mutant

PbGRASP-KO plasmids was constructed with the *E. coli* cloning vector pDEF. hDHFR in the plasmid is the selection marker for the selection of mutant parasite. Homologous sequence arms, the 5' and 3' UTRs were amplified from *P. berghei* gDNA by PCR. Through homologous recombination, the PbGRASP gene was replaced by the human dihydrofolate reductase selection marker. Primers 5 and 6, flanking the 5' UTR, and Primers 7 and 8, flanking the 3' UTR, were used to confirm the presence of the hDHFR cassette in transfected parasites.

Figure 7

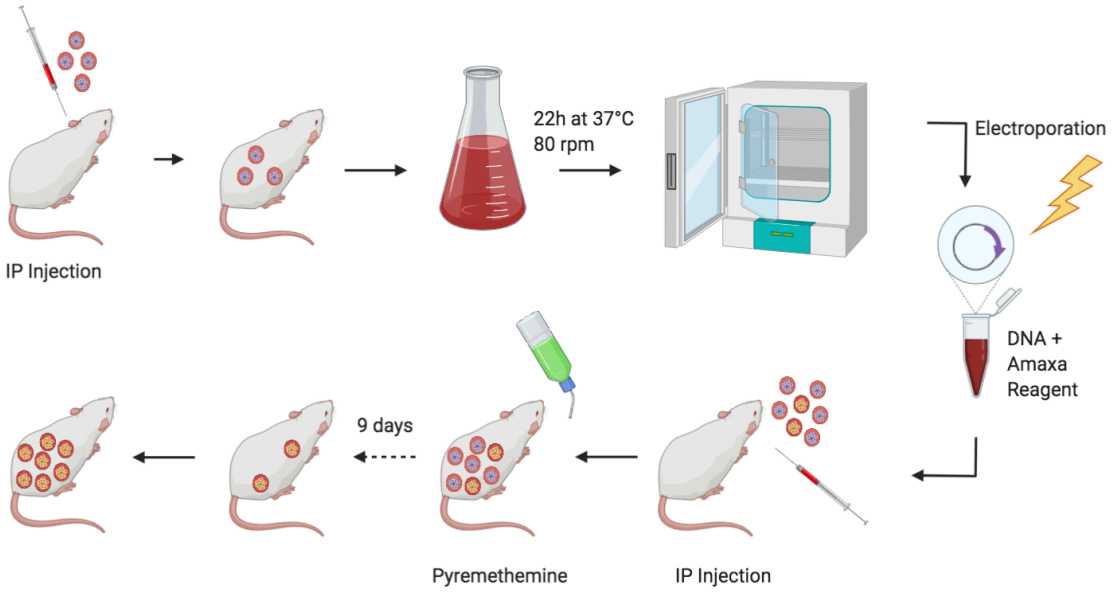

Figure 7 - Generation of PbGRASP-KO parasites through transfection
Naïve female Swiss-Webster mice were intraperitoneally infected with WT *P. berghei* ANKA parasites. When parasitemia reached 3-4% a cardiac puncture was performed, and blood was transferred to culture in 1640 RPMI culture medium for 22 hours at 37°C with a constant shaking at 80 rpm. The recombinant plasmid DNA and the AMAXA reagent were introduced to the parasite culture and subjected to electroporation. The transfected parasite containing WT and PbGRASP-KO mutants, were intraperitoneally infected into naïve mice. The mice were treated with Pyrimethamine for nine days to kill remaining WT parasites and select the PbGRASP-KO strain.

Figure 8

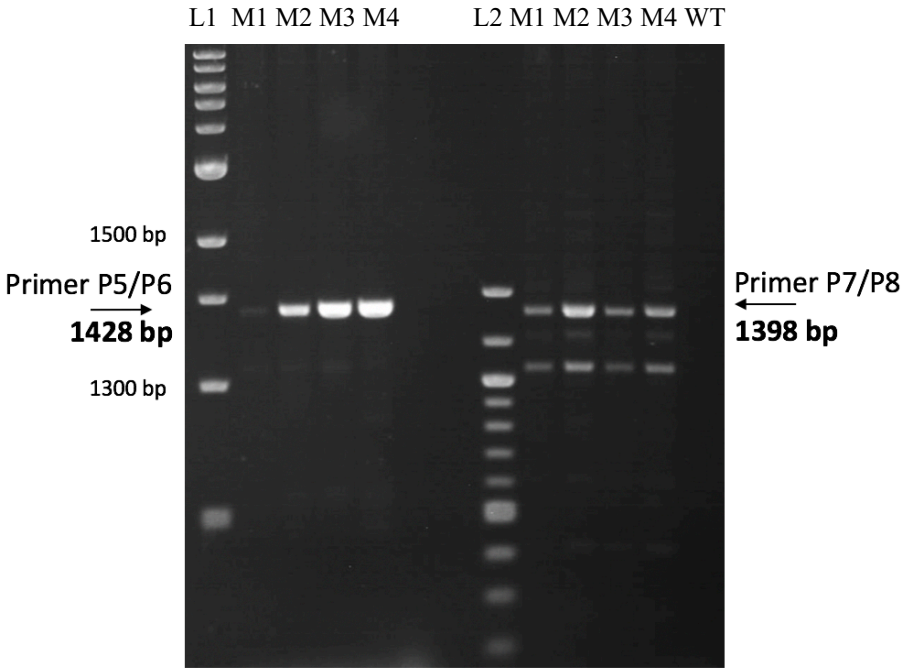

Dr. Tejram Sahu - Unpublished

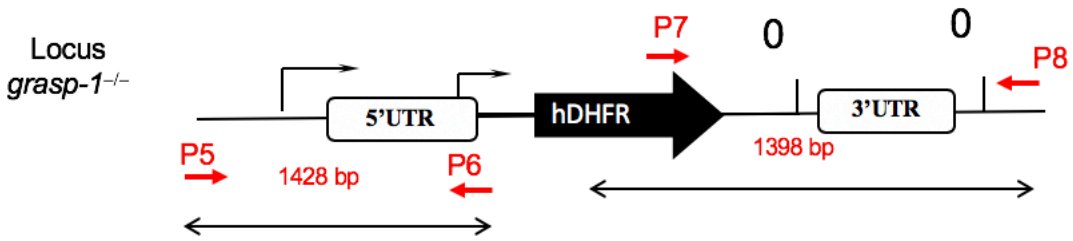

Figure 8 - PCR confirmation of PbGRASP-KO
Following the generation of the PbGRASP-KO strain through transfection, PCR of saponin lysed blood containing erythrocytic forms of the parasites was used to confirm the presence of the hDHFR cassette in samples from 4 infected mice. Primers 5 and 6 amplified a 1428 bp region that overlapped the 5'UTR and the hDHFR cassette. Primers 7 and 8 amplified a 1398 bp region overlapping the 3' UTR and the hDHFR cassette. PCR products were run by gel electrophoresis. All four mice were confirmed to be positively infected by the PbGRASP-KO mutant. Genomic DNA from a WT infected mouse was used as control and showed no PCR amplification. L1: 1 kb DNA ladder, L2: 100 bp DNA ladder, M1-M4: Mouse receiving transfected parasite. WT: Wild type.

Figure 9

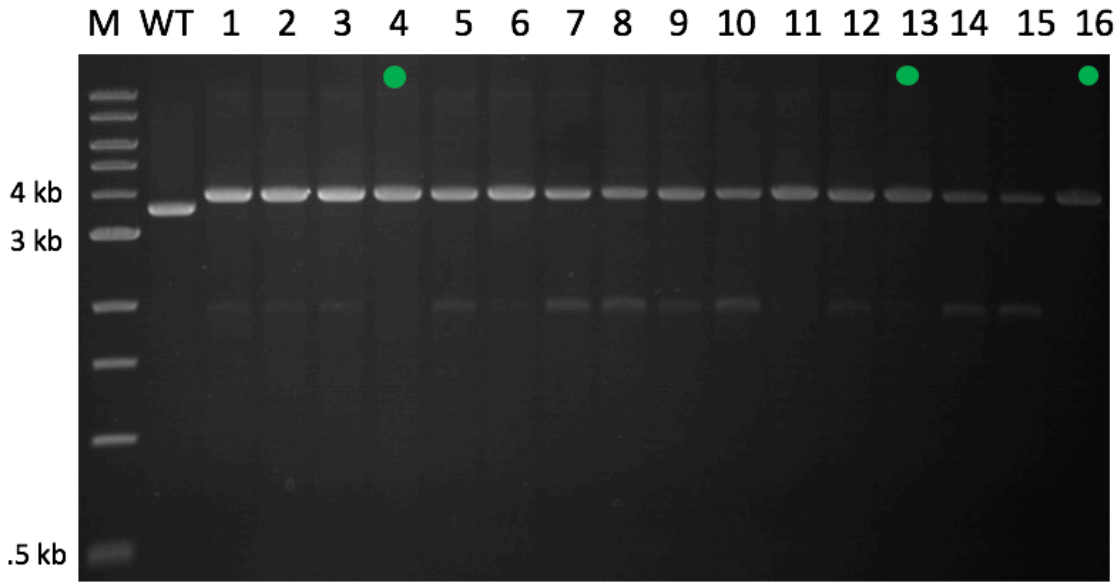

Dr. Tejram Sahu - Unpublished

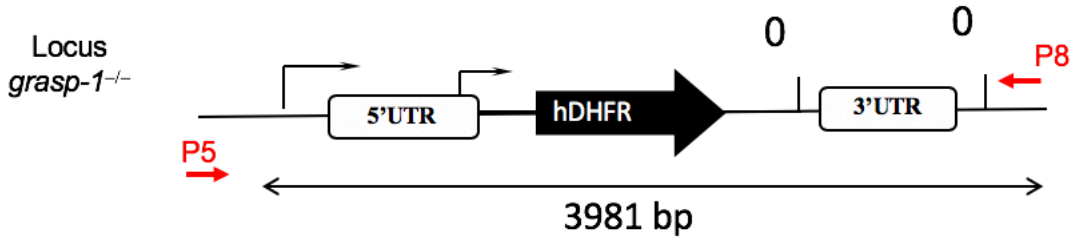

Figure 9 - Generation of PbGRASP-KO blood stage clones
Fifty Swiss-Webster mice were infected with the PbGRASP-KO strain, receiving an infection dose of 0.5 parasites per mouse. 16 mice were initially confirmed to be infected by blood smear. Primers 5 and 8 were chosen to amplify a 3981 bp region from the 5' UTR to the 3' UTR. PCR products were run by gel electrophoresis. All 16 mice were positively confirmed by PCR to be infected with the PbGRASP-KO mutant parasite. The green dots pinpoint the clones (4, 13, 16) that were selected for further characterization because no nonspecific PCR bands were observed. M: 1 Kb DNA ladder.

Figure 10

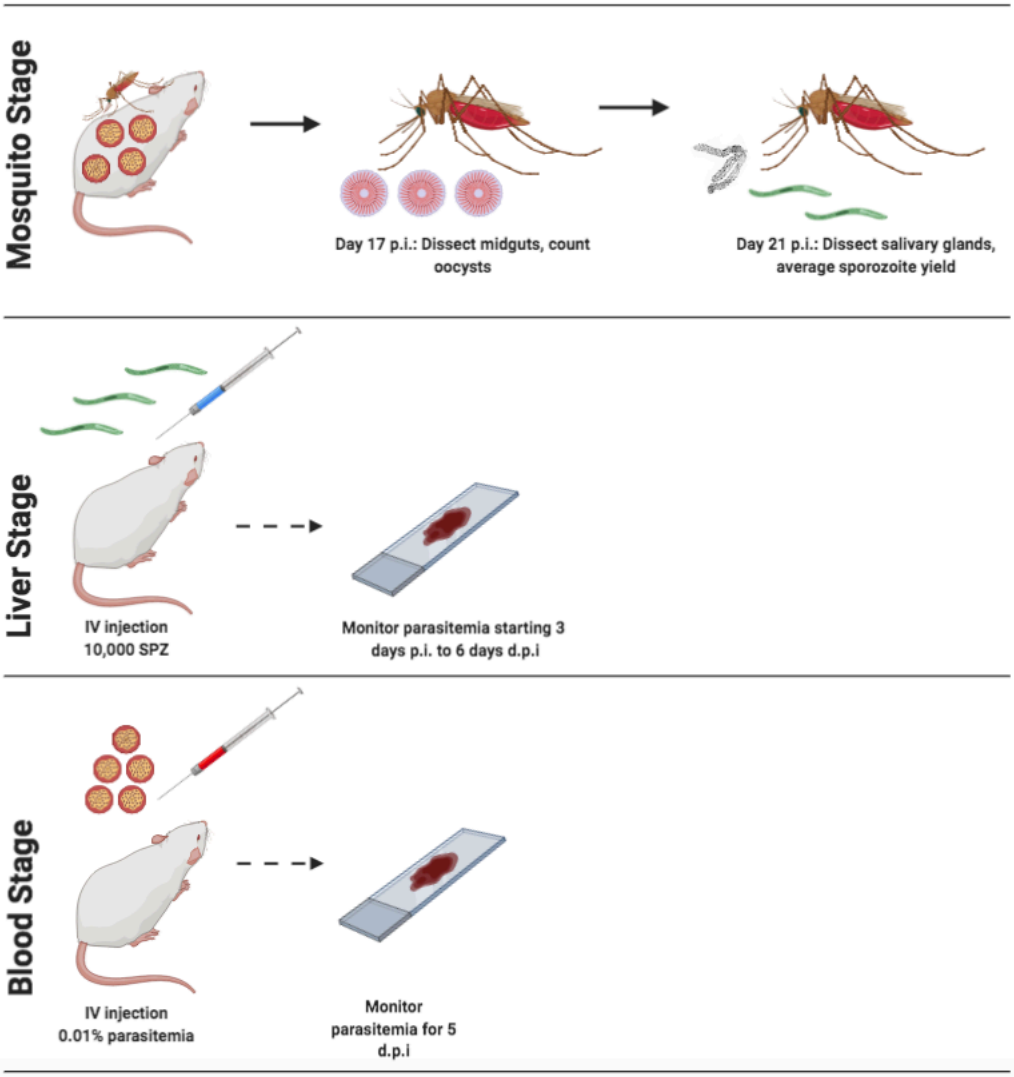

Figure 10 - Methodology to phenotype the blood, mosquito, and liver stage development of *P. berghei*

Mosquito Stage: Two groups of *Anopheles stephensi* mosquitos were infected through blood feeding on WT or PbGRASP-KO infected mice. On day 17 p.i., mosquito midguts were dissected, and oocyst yields were quantified through light microscopy. On day 23 p.i., salivary glands were dissected and the average sporozoite yield per mosquito was quantified. **Liver Stage:** WT and PbGRASP-KO infected *An. stephensi* were dissected, isolating the sporozoites. Two groups of naïve mice were infected (n=5) with WT or a PbGRASP-KO clone. Beginning on day 3 p.i. until day 6 p.i., blood stage parasitemia was measured by Giemsa stained blood smears. **Blood Stage:** Naïve female Swiss-Webster mice were split into two groups of 5 (n=5) and intravenously infected with 0.01% (final parasitemia) of *P. berghei* parasites or a PbGRASP-KO mutant clone. Starting at day 2 p.i. until day 5 p.i., parasitemia was measured by Giemsa stained blood smears.

Figure 11

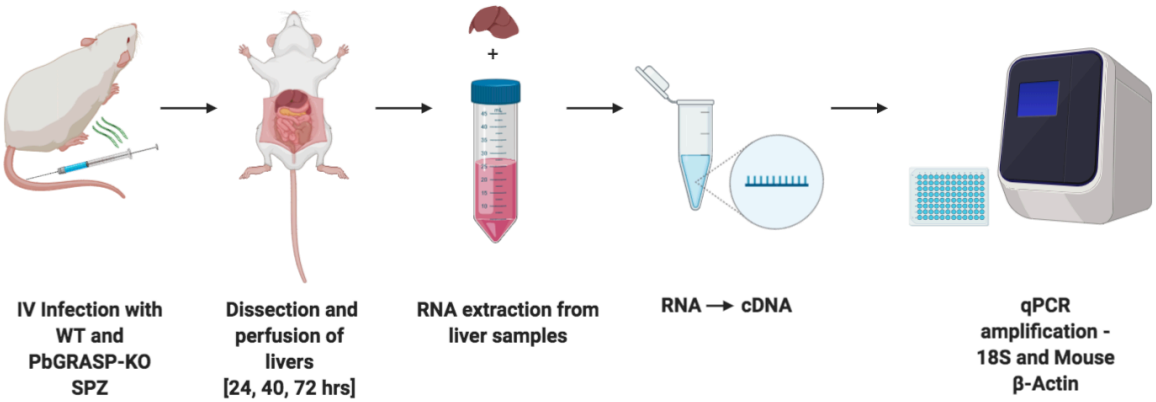

Figure 11 - Quantification of liver stage parasite burden of PbGRASP-KO by qRT-PCR

Three groups of naïve female Swiss Webster (n=5) mice were infected through the tail vein with 10,000 sporozoites of WT or PbGRASP-KO. At 24, 40, or 72-h p.i., mice were anesthetized and dissected. Liver samples were placed in TRIzol and homogenized to isolate RNA. Complementary DNA (cDNA) was synthesized from the RNA isolates and used for qPCR amplification of the 18S ribosomal gene, representing *P. berghei* infection, and Mouse β-actin to normalize data.

Figure 12

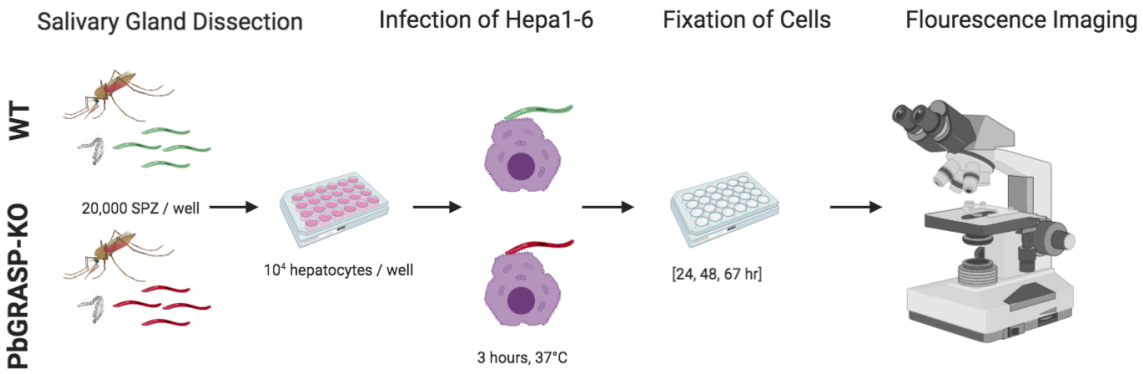

Figure 12 - Phenotyping the liver stage development of PbGRASP-KO in vitro by IFA
Two groups of *An. stephensi* mosquitoes were infected with either WT or a PbGRASP-KO clone. Mosquitoes were dissected on day 21 p.i. Three 24 well plates with glass coverslips, representing 24, 48, and 67-h p.i., were seeded with 100,000 Hepa1-6 cells for WT and PbGRASP-KO infection, in triplicate. 20,000 sporozoites were incubated per well for 3-h at 37°C, 5% CO_2. At 24, 48, and 67-h p.i., wells were fixed. The cells were imaged through fluorescence microscopy, labeled with rabbit anti-TRAP, rat anti-ATG8, mouse anti-HSP70 antibodies, corresponding Alexa conjugated secondary antibodies, and DAPI.

Figure 13

A.

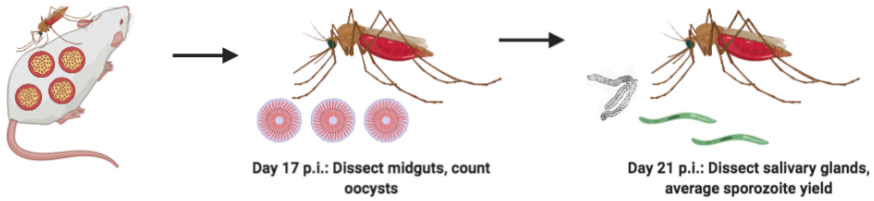

B.

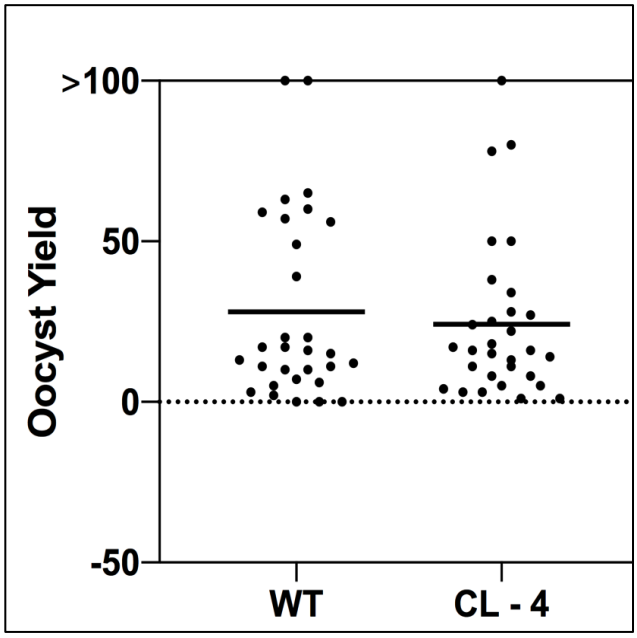

Group (n = 30)	Average Sporozoites per Female Mosquito
WT	14, 375
CL-4 GRASP KO	20,125
CL-16 GRASP KO	19,100

Figure 13 - Growth of PbGRASP-KO strain in mosquito stage development
A. On day 17 p.i., *A. stephensi* mosquitoes infected with WT or PbGRASP-KO were dissected and the midguts were isolated and stained to quantify oocysts. There was no significant difference in oocyst numbers between WT and PbGRASP-KO Cl 4.
B. On day 21 p.i., mosquitoes from the same infection groups were dissected and the salivary glands were isolated to quantify the average number of sporozoites per female mosquito. No significant difference in sporozoite yield of WT and PbGRASP-KO clones 4 and 16 was observed.

Figure 14

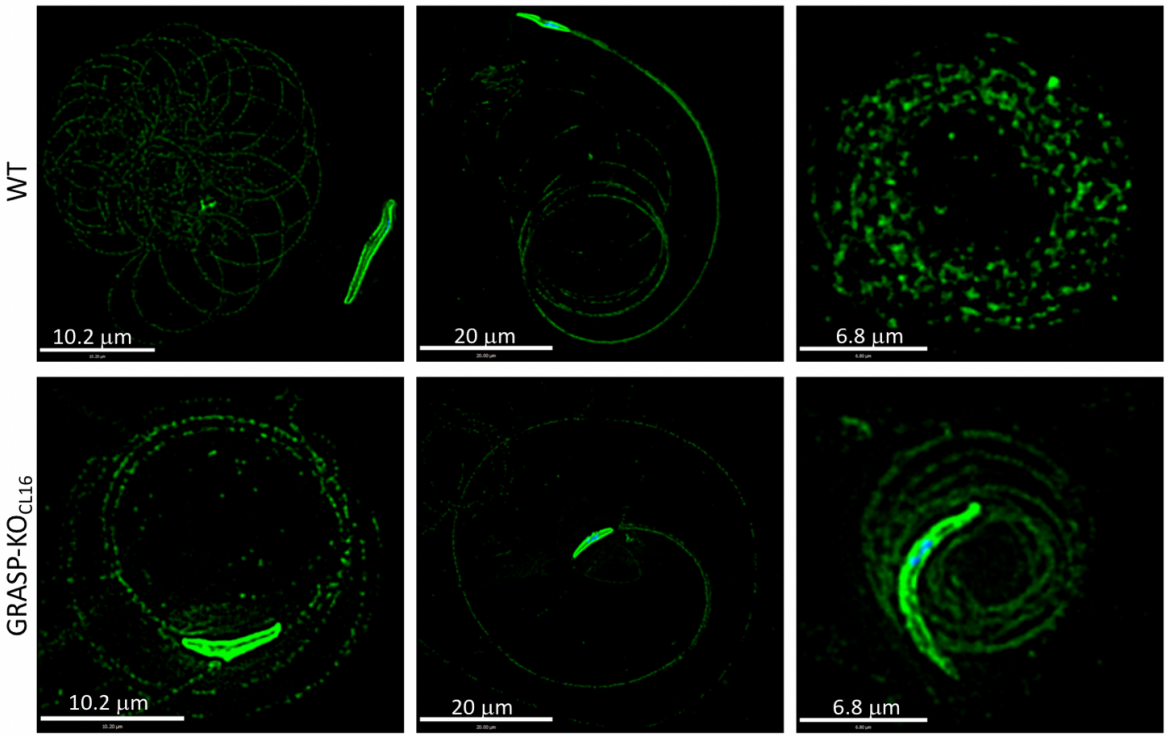

Dr. Tejram Sahu - Unpublished

Figure 14 - Motility of PbGRASP-KO sporozoite
Sporozoite gliding ability is observed through fluorescence microscopy. CSP, a sporozoite surface protein that facilitates motility, is left behind on the plastic surface during sporozoite gliding. CSP trails were fixed and stained with an anti-CSP antibody (green). Both the WT and PbGRASP-KO parasite left similar trails of CSP.

Figure 15

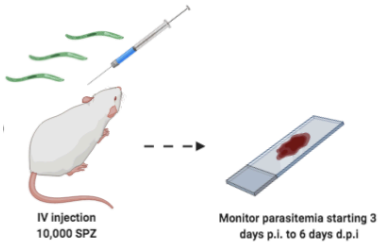

A.

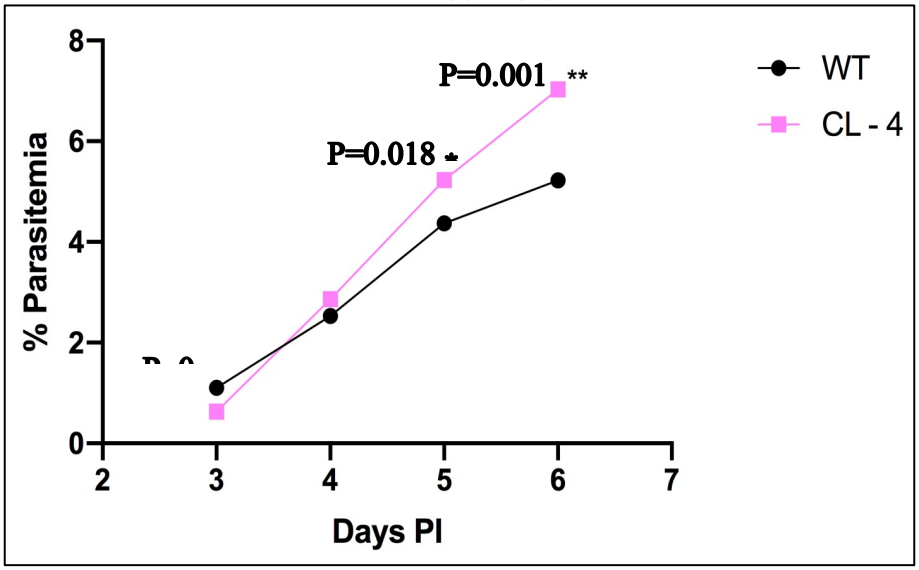

B.

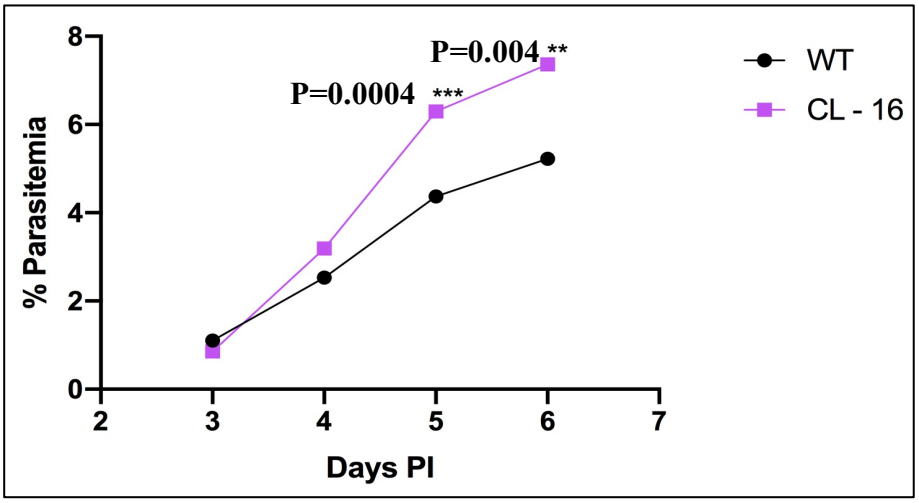

Figure 15 - Blood stage infection after PbGRASP-KO sporozoite infection
Two groups of naïve Swiss-Webster mice (n=5) were injected with 10,000 WT or PbGRASP-KO sporozoites. Parasitemia in the blood was measured from day 3 to 6 p.i., quantified by Giemsa blood smears. Erythrocytic forms of WT and PbGRASP-KO began emerging on day 3. Although not statistically significant, fewer PbGRASP-KO parasites were quantified than WT 3 days p.i. On day 4, the PbGRASP-KO parasitemia surpassed WT. The increased PbGRASP-KO infection was statistically significant on day 5 p.i. (**A**: p=0.018, **B**: p=0.0004). On day 6 p.i., the PbGRASP-KO parasitemia was significantly higher from the WT (**A**: p=0.001, **B**: p=0.004).

Figure 16

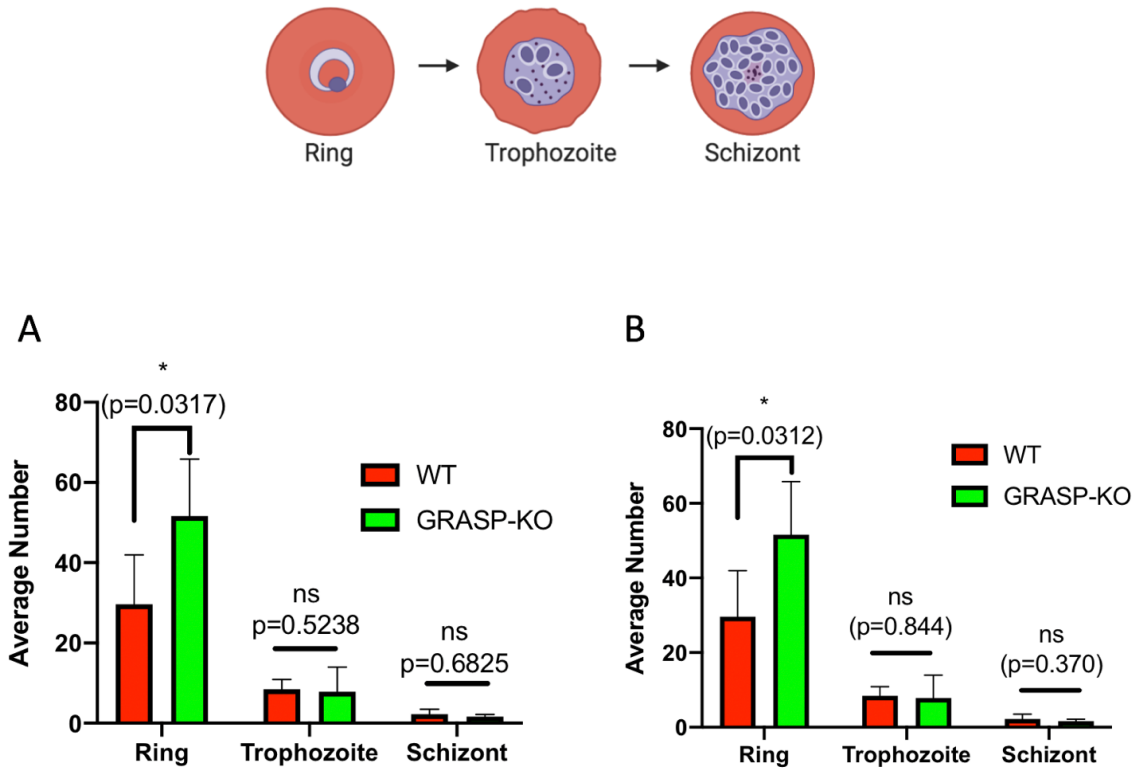

Figure 16 - Blood stage composition of WT and PbGRASP-KO after sporozoite infection

To inspect blood stage forms of the WT and PbGRASP-KO at day 4 and 5 p.i., Giemsa stained blood smears were observed using light microscopy and the diverse blood stages were quantified by counting 25 fields per blood smear. (A) Comparative analysis of different blood stages on day-4 p.i. (B) Comparative analysis of different blood stages on day-5 p.i. Analysis of PbGRASP-KO clone 16 showed a statistically greater number of rings compared to WT and fewer trophozoite forms compared to WT at day 4 and 5 p.i. Data represents Mean ± SD of data from 5 mice in each group.

Figure 17

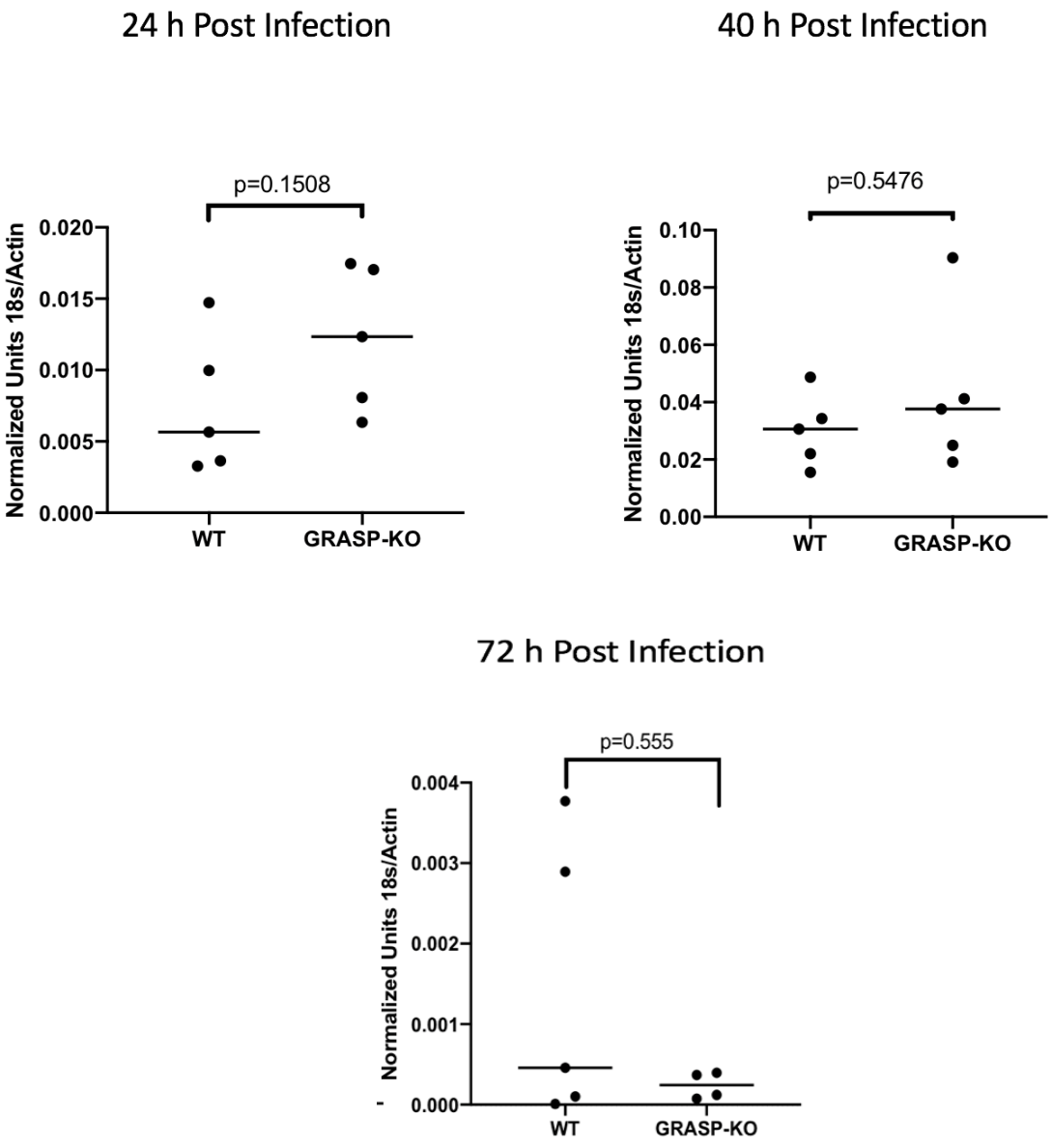

Figure 17 - Quantitative RT-PCR of parasite gene expression in liver stage
Liver stage parasite burden of PbGRASP-KO (n=5) and WT (n=5) parasite infected Swiss Webster mice were quantified by qRT-PCR at 24, 40, 72-h p.i. 18S, a ribosomal gene, was selected to measure parasite gene expression in liver samples. Mouse β-actin was selected to normalize the parasite 18S expression. No difference in gene expression between WT and PbGRASP-KO was observed at any time point. PCR was done in triplicate for each liver sample for each gene. Data represent Mean ± SD. Mann-Whitney statistical test was performed to determine the level of significance.

Figure 18

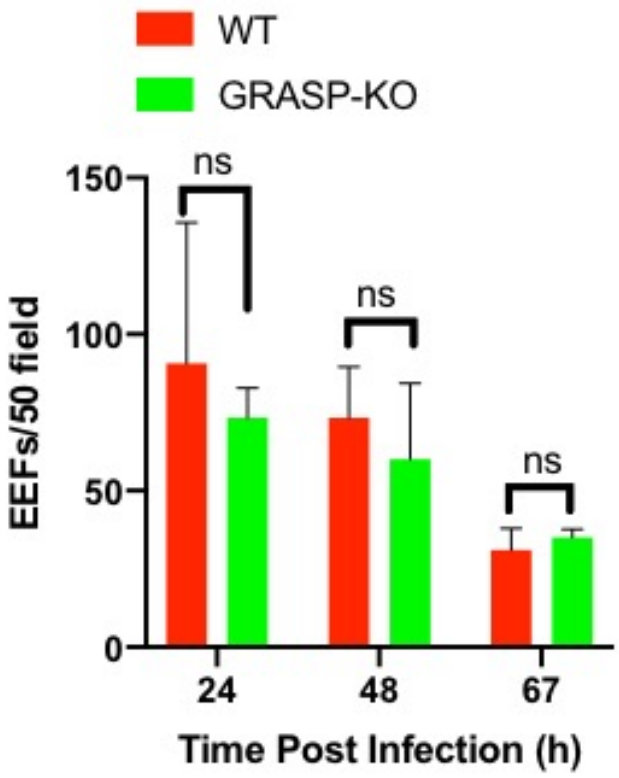

Figure 18 - Quantitative estimation of liver stage infection by WT and PbGRASP-KO
A PbGRASP-KO and WT infection of Hepa1-6 cells at 24, 48, and 67-hrs p.i. was observed by fluorescence microscopy. Quantification of the exoerythrocytic forms (EEFs) of the parasite was obtained by counting parasites identified by HSP70 staining per 50 fields at each time point per coverslip. Data represent Mean ± SD of experiment done in triplicate.

Figure 19

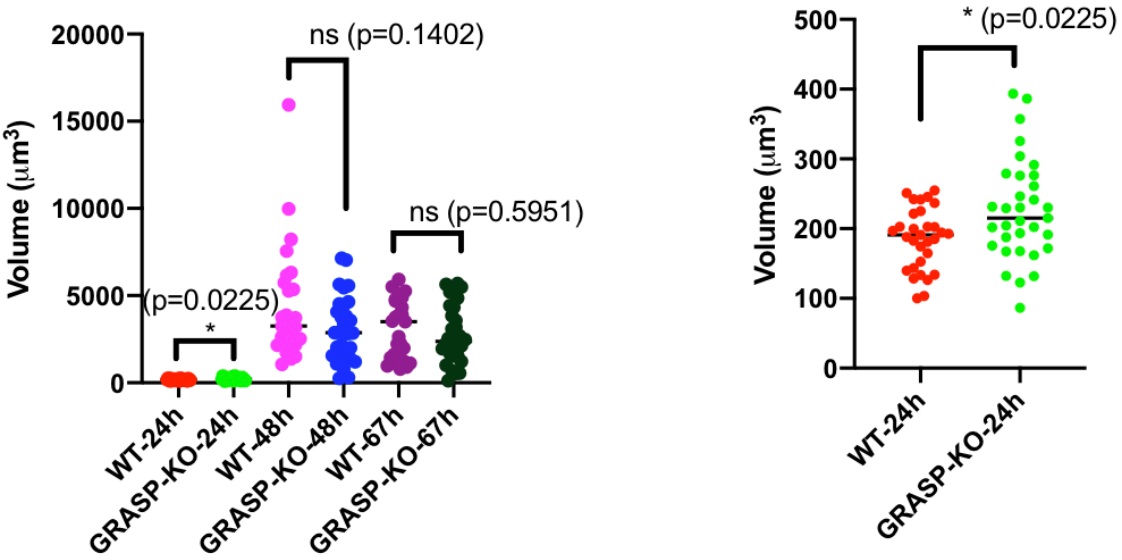

Figure 19 - Volume quantification of EEFs over time
A PbGRASP-KO and WT infection of Hepa1-6 cells at 24, 48, and 67-hrs p.i. was observed by fluorescence microscopy. Volocity software deconvolved images tagged with HSP70 fluorescence to obtain the average volumic area (volume) of WT and PbGRASP-KO (n=35) images at 24, 48, and 67-hrs p.i. At 24-h p.i., the PbGRASP-KO group was statistically significant from WT with a larger volume. At 48, 67-hrs. WT and PbGRASP-KO volumes were not significant from each other. Data represent Mean ± SD.

Figure 20

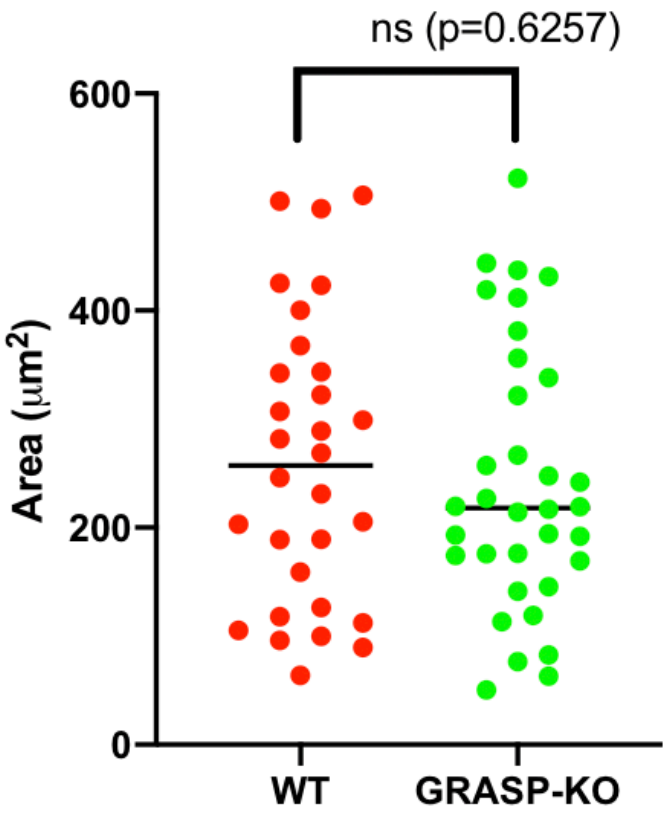

Figure 20 - Size of EEFs at 67-h p.i.
A PbGRASP-KO and WT infection of Hepa1-6 cells at 67-h p.i. was observed by fluorescence microscopy. Images were deconvolved through Volocity Software and HSP70 staining was used to obtain the average area (µm^2) of the two strains (n≥30). The difference between WT and PbGRASP-KO area was not significant between the two strains. Data represent Mean ± SD.

Figure 21

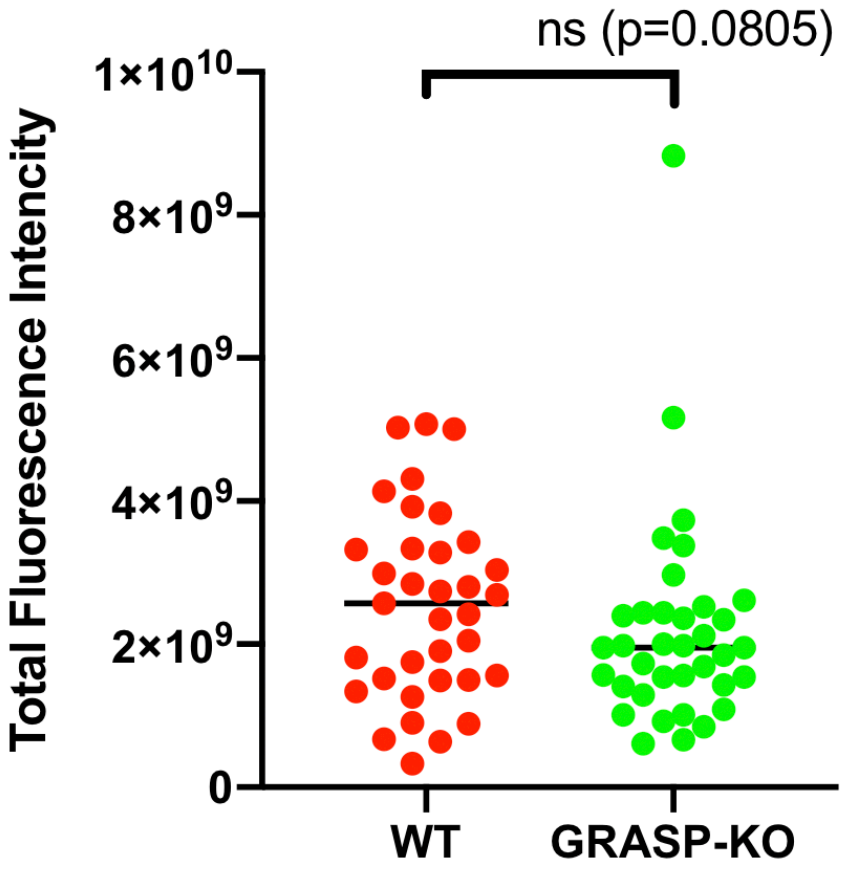

Figure 21 - Indirect measurement of nucleic acid content of liver forms at 48-h p.i.
A PbGRASP-KO and WT infection of Hepa1-6 cells at 48-hrs p.i. was observed by fluorescence microscopy. Images were deconvolved through Volocity Software and DAPI fluorescence overlapping with HSP70 fluorescence was used to obtain the total fluorescence intensity of the two strain's (n=35) nucleic matter at 48-hrs p.i. The difference between WT and PbGRASP-KO total DAPI fluorescence intensity was not significant between the two strains. Data represents Mean ± SD.

Figure 22

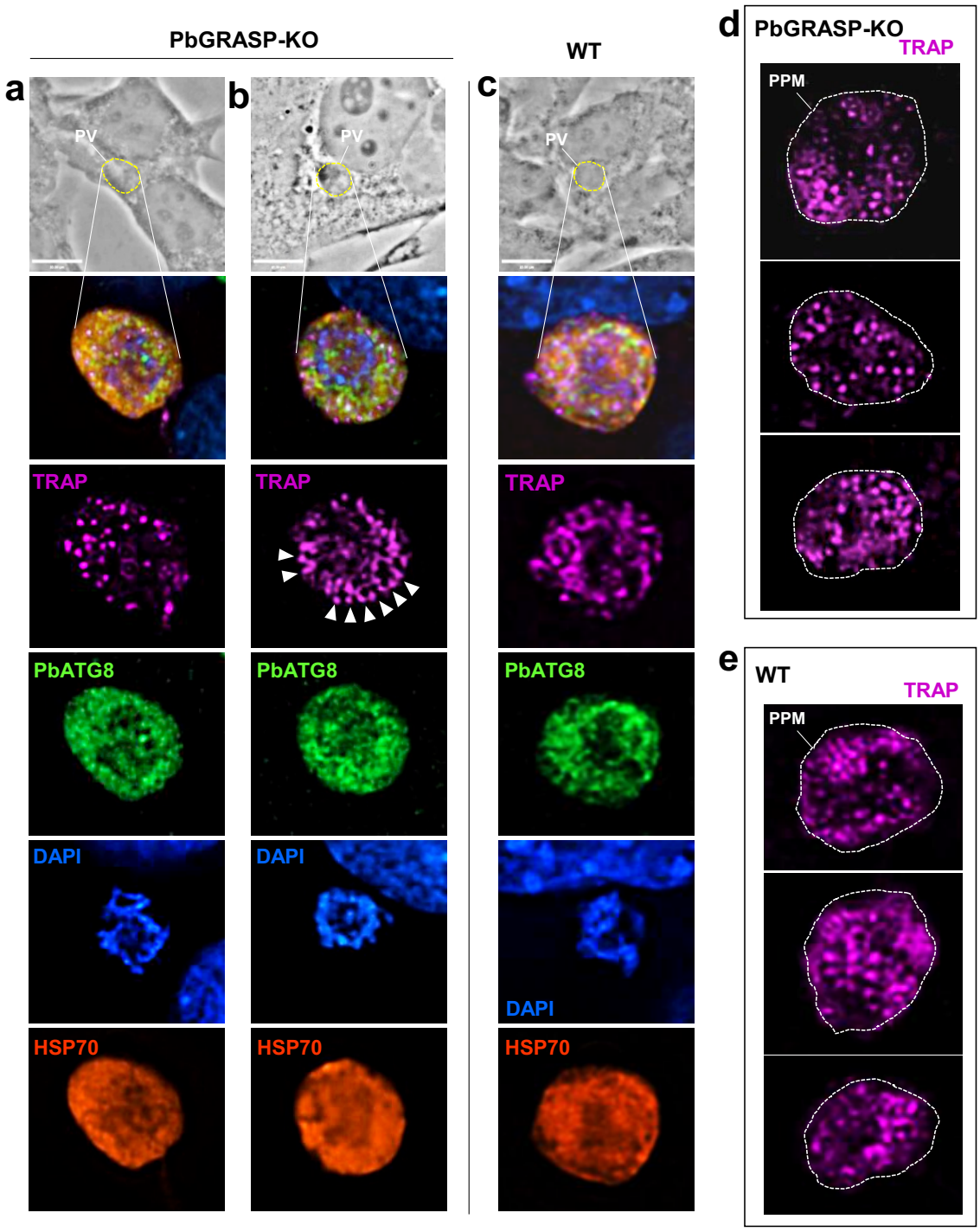
PbGRASP-KO
WT
a
b
c
d
e
PV
PV
PV
TRAP
TRAP
TRAP
PbATG8
PbATG8
PbATG8
DAPI
DAPI
DAPI
HSP70
HSP70
HSP70
PbGRASP-KO
TRAP
PPM
WT
TRAP
PPM

Figure 22 - Morphology of PbGRASP-KO liver forms at 24-h p.i.
A PbGRASP-KO and WT infection of Hepa1-6 cells at 24-h p.i. is observed by fluorescence microscopy. Micronemes (TRAP), the apicoplast/autophagic structures (PbATG8), nucleus (DAPI) and cytoplasm (HSP70) show microneme compartmentalization in PbGRASP-KO (**panels a** and **b**) similar to WT parasites (**panel c**). **Panel b** depicts clustering of micronemes (TRAP) beneath the parasite plasma membrane, (emphasized by arrowheads). **Panels d** and **c** show more examples of microneme (TRAP) clustering within the cytoplasm of the two strains. PPM, parasite plasma membrane. All bars, 10 microns.

Figure 23

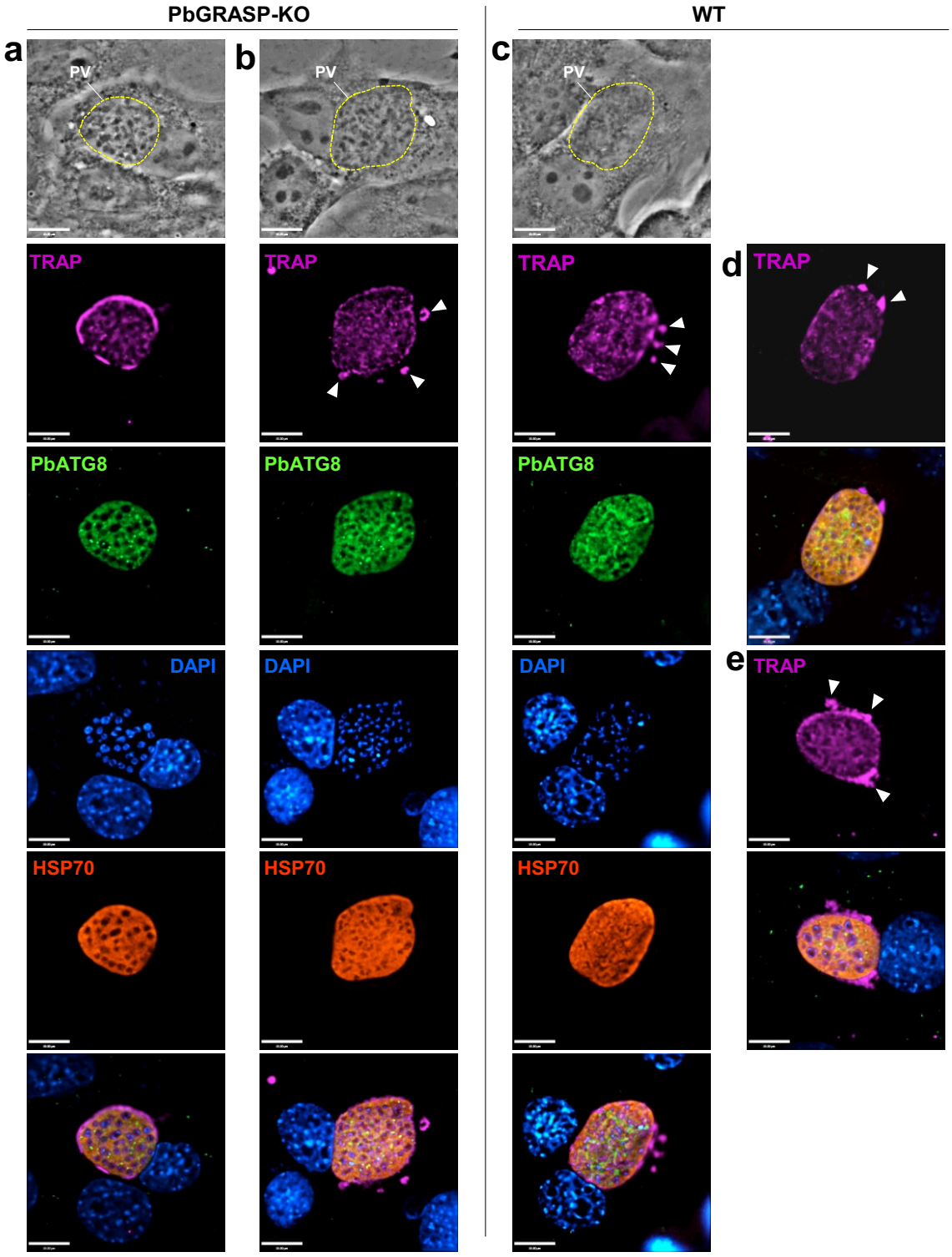

Figure 23 - Morphology of PbGRASP-KO liver forms at 48hour p.i.
A PbGRASP-KO and WT infection of Hepa1-6 cells at 48-h p.i. observed by fluorescence microscopy. Micronemes (TRAP), the apicoplast/autophagic structures (PbATG8), nucleus (DAPI) and cytoplasm (HSP70) showing representative examples of a small PV (**panel a**) and a large PV (**panel b**) for PbGRASP-KO. **Panel a** illustrates an intense TRAP staining beyond the HSP70 signal within the PV space. In **panel b**, the TRAP staining become fainter within the KO, similarly to WT parasites (**panel c**). Interestingly, the TRAP signal was also observed distant from the parasite plasma membrane (emphasized by the arrowheads). **Panels d** and **e** show more examples of TRAP staining for WT parasites. The TRAP signal could correspond to micronemes discarded into the PV, within evaginations emanating from the PVM, or expulsion of micronemes beyond the PV, thus in the host cytosol. All bars, 10 microns.

Figure 24

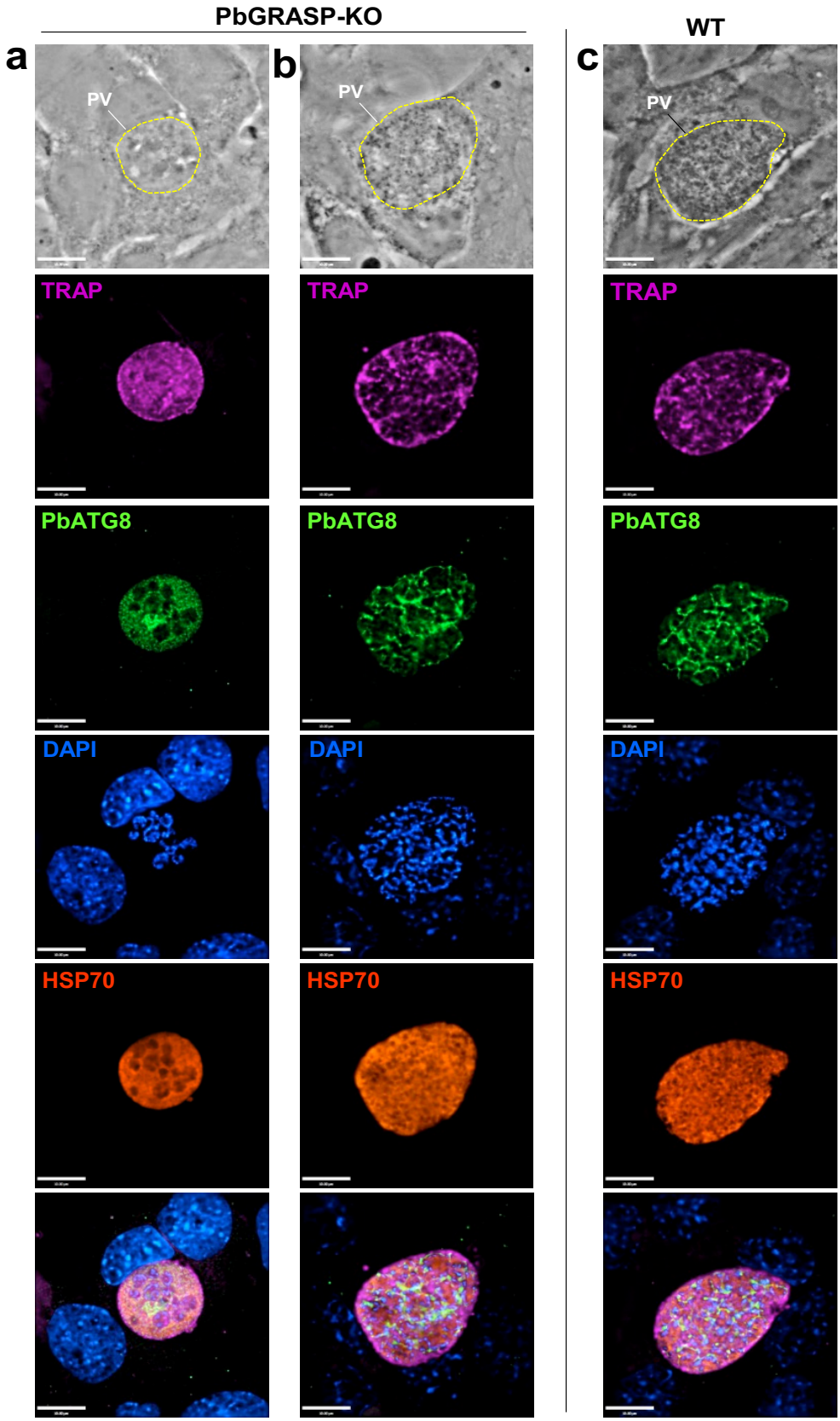
PbGRASP-KO
WT
a
b
c
PV
PV
PV
TRAP
TRAP
TRAP
PbATG8
PbATG8
PbATG8
DAPI
DAPI
DAPI
HSP70
HSP70
HSP70

Figure 24 -Morphology of PbGRASP-KO liver forms at 67-h p.i.
A PbGRASP-KO and WT infection of Hepa1-6 cells at 67-h p.i. observed by fluorescence microscopy. Micronemes (TRAP), the apicoplast/autophagic structures (PbATG8), nucleus (DAPI) and cytoplasm (HSP70) showing representative examples of an underdeveloped PV (**panel a**) and a large PV (**panel b**) for PbGRASP-KO. The small PV in **panel a** is characterized by a strong residual TRAP staining in the mutant cytoplasm while the PV in **panel b** is similar to the WT PV (**panel c**). In both strains, ATG8 was re-associated with the apicoplast forming a branched network at 67 h p.i. All bars, 10 microns.

Figure 25

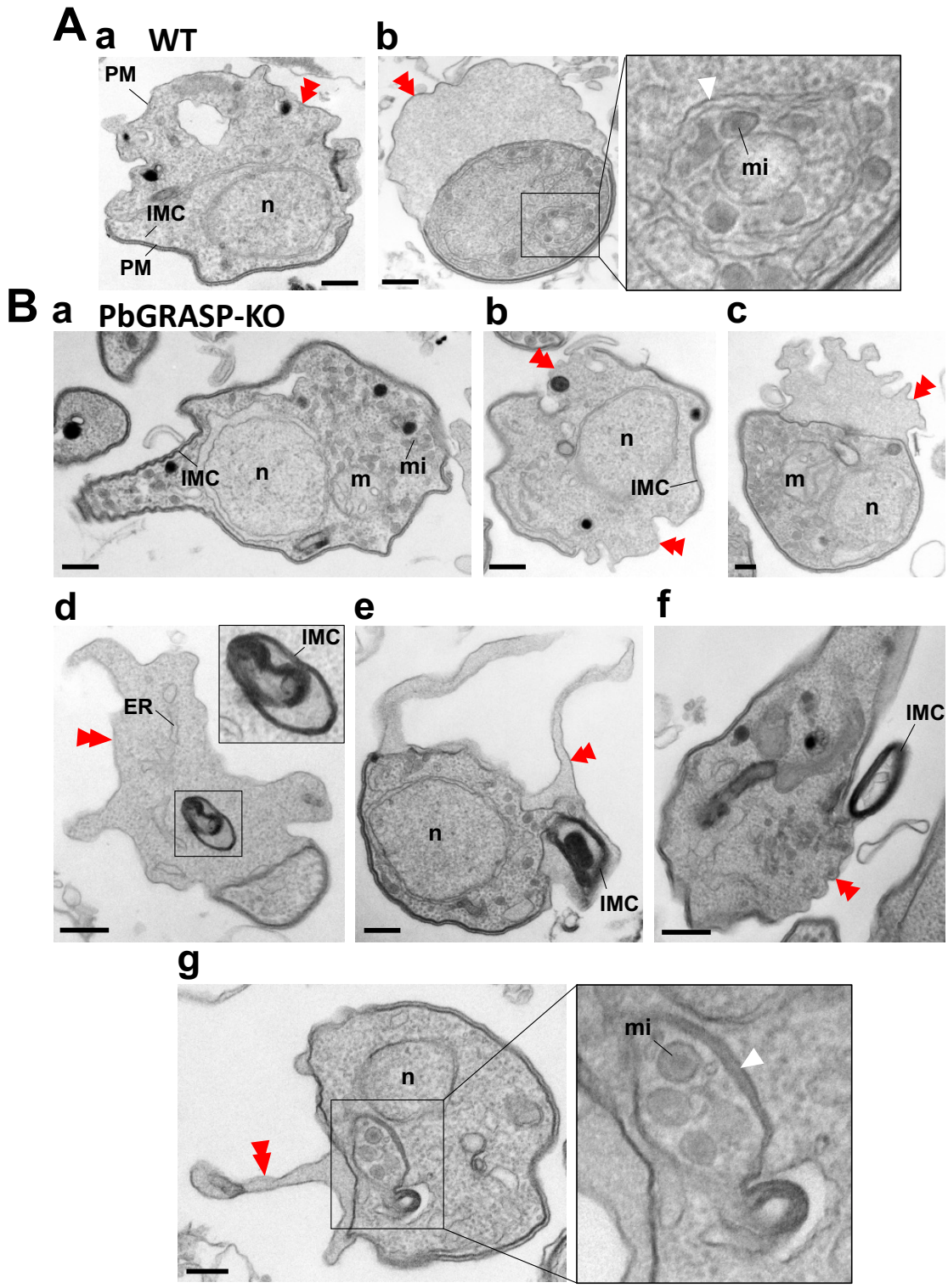
A
a
WT
PM
IMC
n
PM
b
mi
B
a
PbGRASP-KO
IMC
n
m
mi
b
n
IMC
c
m
n
d
IMC
ER
e
n
IMC
f
IMC
g
n
mi

Figure 25 - Ultrastructure of axenic GRASP-deficient *P. berghei* sporozoites
EM of 12h-converting sporozoites from WT *P. berghei* (**A**) or GRASP-deficient *P. berghei* (**B**) showing similar features during conversion. In A, **panel a** illustrates the detachment of the inner membrane complex (IMC) from the plasma membrane (PM), allowing the overgrowth of the cytoplasm. Double arrows point to areas devoid of submembrane IMC. **Panel b** shows a clustering of micronemes (mi) within a double sac membrane (white arrow) magnified in the inset. In B, **panels a** to **c** show the remodeling of the IMC in the knockout, with progressive dismantling of this organelle from the plasma membrane (double arrows) similar to WT parasites. **Panel d** illustrates the compaction of IMC into membrane whorls in the cytoplasm (inset), followed their transport to the plasma membrane (**panel e**) and then expulsion from the parasite (**panel f**). **Panel g** shows the sequestration of micronemes in a double membrane structure (arrows). m, mitochondrion; n, nucleus. All bars, 200 nm.

Figure 26

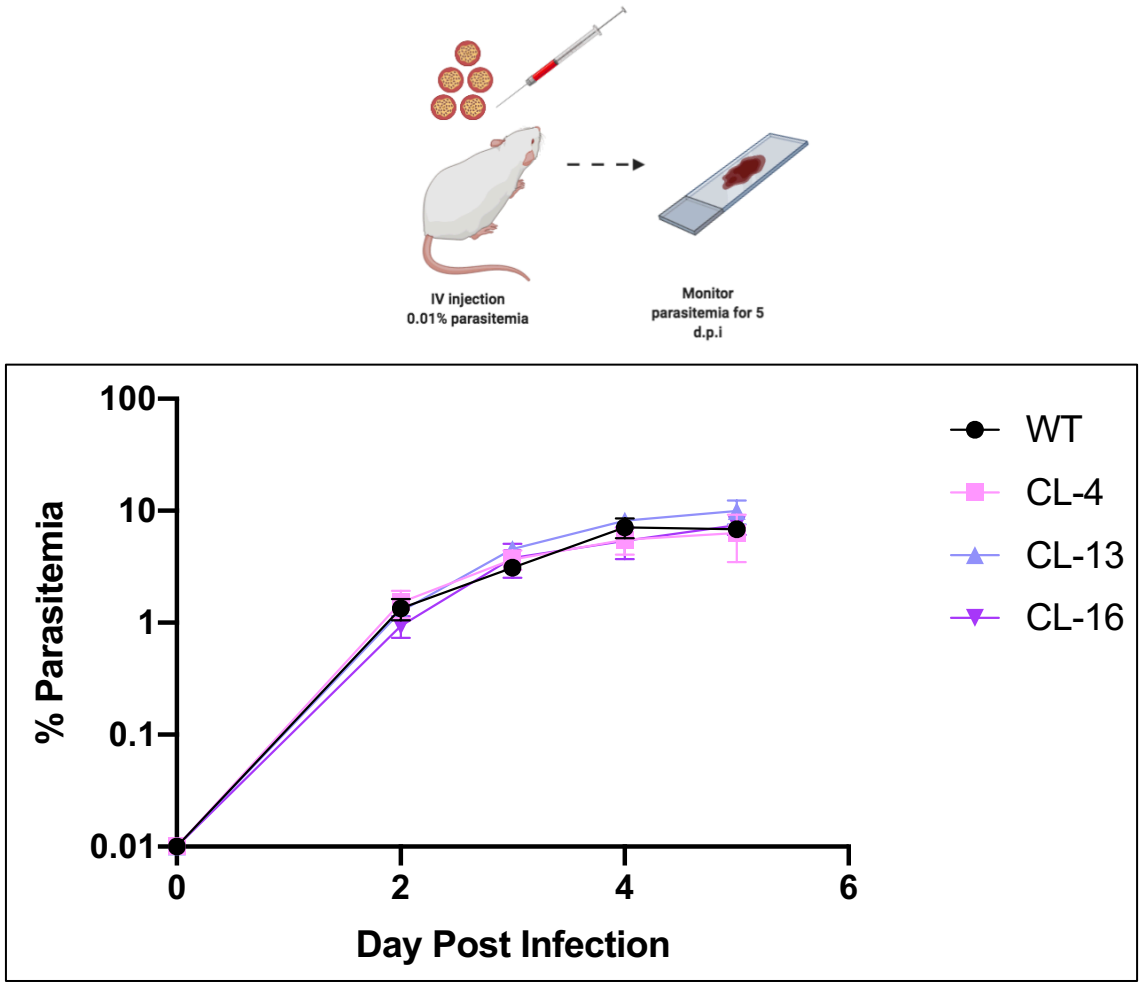

Figure 26 - Blood stage development of PbGRASP-KO strain
Two groups of naïve Swiss-Webster mice (n=5) were injected with a final 0.01% WT or PbGRASP-KO infected blood. Parasitemia was measured from day 2 to 6 p.i., quantified by Giemsa stained thin blood smears. We observed that PbGRASP-KO clones (4, 13, 16) developed identical to the WT infection across all measured time points.

Figure 27

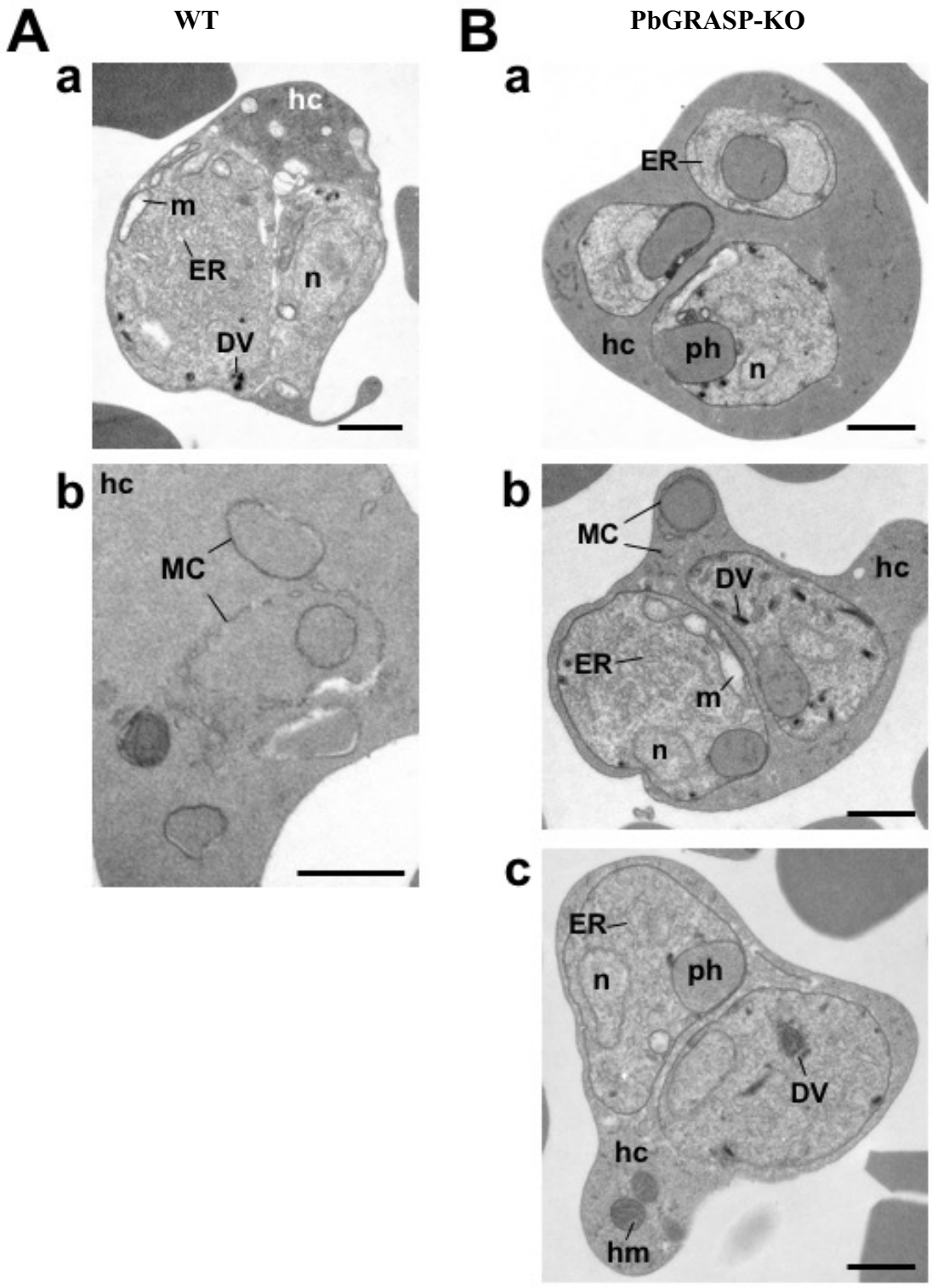
A
WT
a
hc
m
ER
n
DV
b
hc
MC
B
PbGRASP-KO
a
ER
hc
ph
n
b
MC
DV
hc
ER
m
n
c
ER
n
ph
DV
hc
hm

Figure 27 - Ultrastructure of GRASP-deficient *P. berghei* blood forms
EM of infected red blood cells from mice infected for 5 days with WT *P. berghei* (**A**) or GRASP-deficient *P. berghei* (**B**) showing no difference in the morphology and organellar content between the two strains. For the knockout, three infected red blood cells are shown, with young stage parasites characterized by large hemoglobin-containing phagosomes (ph) (**B, panel a**); a more advanced parasite stage in which Maurer's clefts (MC) are formed in host cell (hc; **B, panel b**) similar to WT parasites (**A, panel b**) and; a later stage characterized by a decline in electron-density of the host cytoplasm, indicative of hemoglobin consumption by growing parasites (**A, panel c**). DV, digestive vacuole with hemozoin; ER, endoplasmic reticulum; m, mitochondrion; hm, host mitochondrion; n, nucleus. All bars, 1 micron.

Chart 1

Reference	Primer Sequence
1.	5’-CCC**AAGCTTGGG**AGTGTTTATATGGTAAATTTTACATTTACATATC-3’
2.	5’-AAAA**CTGCAG**CTATATCCTTAAAAGGAAAATAAATATACGGTGT-3’
3.	5’-CGG**GGTAC**CCCGATGAATTGATTGGGGATAAATAAAACTACG-3’
4.	5’-G**GAATTCC**TATATATCCATTTTTCCTCTTCACAAAAGTAATTAC-3’
5.	5’-AAGGGAAAGTTATATTTTTTTAGTAACTGGAGT-3’
6.	5’-ATGCTTAAGTTTACAATTTAATATTCATACTTTAAGTA-3’
7.	5’-GTGCATGCACATGCATGTAAATAG-3’
8.	5’-TCACATAATTATATAGTTAGCTAATATTACTCT-3’
9.	F: 5’-AAGCATTAAATAAAGCGAATACATCCTTAC-3’
10.	R: 5’-GGAGATTGGTTTTGACGTTTATGTG-3’
11.	F: 5’-GGCTGTATTCCCCTCCATCG-3’
12.	R: 5’-CCAGTTGGTAACAATGCCATGT-3’

Bold text reflects restriction enzyme cut sites*

References

1. Organization WH. 2019. World Malaria Report 2018. Geneva: World Health Organization.
2. Crawley, J, C Chu, G Mtove, and F Nosten. 2010. "Malaria in Children." *The Lancet* 375 (9724): 1468–81. doi:10.1016/S0140-6736(10)60447-3.
3. Fairhurst, R, and A Dondorp. 2016. "Artemisinin-Resistant Plasmodium Falciparum Malaria." *Microbiology Spectrum* 4 (3). doi:10.1128/microbiolspec.ei10-0013-2016.
4. Ashley, E, M Dhorda, R Fairhurst, C Amaratunga, P Lim, and S Suon. 2014. "Spread of Artemisinin Resistance in Plasmodium Falciparum Malaria." *New England Journal of Medicine* 371 (8): 786–86. doi:10.1056/nejmx140047.
5. Elvidge, S. 2015. "First Malaria Vaccine Receives Positive Scientific Opinion from EMA." *The Pharmaceutical Journal*, July. doi:10.1211/pj.2015.20069061.
6. Gosling R, von Seidlein L. 2016. The Future of the RTS,S/AS01 Malaria Vaccine: An Alternative Development Plan. *PLOS Medicine*. April. doi:10.1371/journal.pmed.1001994.
7. Jayabalasingham, B, N Bano, and I Coppens. 2010. "Metamorphosis of the Malaria Parasite in the Liver Is Associated with Organelle Clearance." *Cell Research* 20 (9): 1043–59. doi:10.1038/cr.2010.88.
8. Spreng, B, H Fleckenstein, P Kübler, C Di Biagio, M Benz, P Patra, U Schwarz, M Cyrklaff, and F Frischknecht. 2019. "Microtubule Number and Length Determine

Cellular Shape and Function in Plasmodium." *The EMBO Journal* 38 (15). doi:10.15252/embj.2018100984.

9. Ménard, R, J Tavares, I Cockburn, M Markus, F Zavala, and R Amino. 2013. "Looking under the Skin: the First Steps in Malarial Infection and Immunity." *Nature Reviews Microbiology* 11 (10): 701–12. doi:10.1038/nrmicro3111.
10. Voss, C, K Ehrenman, G Mlambo, S Mishra, K Kumar, J Sacci, P Sinnis, and I Coppens. 2016. "Overexpression of Plasmodium Berghei ATG8 by Liver Forms Leads to Cumulative Defects in Organelle Dynamics and to Generation of Noninfectious Merozoites." *MBio* 7 (3). doi:10.1128/mbio.00682-16.
11. Matz, J, and K Matuschewski. 2018. "An in Silico down-Scaling Approach Uncovers Novel Constituents of the Plasmodium-Containing Vacuole." *Scientific Reports* 8 (1). doi:10.1038/s41598-018-32471-6.
12. Spielmann, T, G Montagna, L Hecht, and K Matuschewski. 2012. "Molecular Make-up of the Plasmodium Parasitophorous Vacuolar Membrane." *International Journal of Medical Microbiology* 302 (4-5): 179–86. doi:10.1016/j.ijmm.2012.07.011.
13. Manjithaya, R, and S Subramani. 2011. "Autophagy: a Broad Role in Unconventional Protein Secretion?" *Trends in Cell Biology* 21 (2): 67–73. doi:10.1016/j.tcb.2010.09.009.
14. Bano, N, J Romano, B Jayabalasingham, and I Coppens. 2007. "Cellular Interactions of Plasmodium Liver Stage with Its Host Mammalian

Cell." *International Journal for Parasitology* 37 (12): 1329–41. doi:10.1016/j.ijpara.2007.04.005.

15. Coppens, I. 2011. "Metamorphoses of Malaria: the Role of Autophagy in Parasite Differentiation." *Essays in Biochemistry*. doi:10.1042/bse0510127.
16. Meis, J, J Verhave, P Jap, and J Meuwissen. 1985. "Transformation of Sporozoites of Plasmodium Berghei into Exoerythrocytic Forms in the Liver of Its Mammalian Host." *Cell and Tissue Research*. doi:10.1007/BF00217180.
17. Vaughan, A, A Aly, and S Kappe. 2008. "Malaria Parasite Pre-Erythrocytic Stage Infection: Gliding and Hiding." *Cell Host & Microbe* 4 (3): 209–18. doi:10.1016/j.chom.2008.08.010.
18. Sturm, A, R Amino, C van de Sand, T Regen, S Retzlaff, A Rennenberg, A Krueger, JM Pollok, R Menard, and VT R, Heussler. 2006. "Manipulation of Host Hepatocytes by the Malaria Parasite for Delivery into Liver Sinusoids." *Science* 313 (5791): 1287–90. doi:10.1126/science.1129720.
19. Soulard, V, H Bosson-Vanga, A Lorthiois, C Roucher, J Franetich, G Zanghi, M Bordessoulles, et al. 2015. "Plasmodium Falciparum Full Life Cycle and Plasmodium Ovale Liver Stages in Humanized Mice." *Nature Communications* 6 (1). doi:10.1038/ncomms8690.
20. Suh, K. 2004. "Malaria." *Canadian Medical Association Journal* 170 (11): 1693–1702. doi:10.1503/cmaj.1030418.
21. Siciliano, G, and P Alano. 2015. "Enlightening the Malaria Parasite Life Cycle: Bioluminescent Plasmodium in Fundamental and Applied Research." *Frontiers in Microbiology* 6 (November). doi:10.3389/fmicb.2015.00391

22. Aly, A, A Vaughan, and S Kappe. 2009. “Malaria Parasite Development in the Mosquito and Infection of the Mammalian Host.” *Annual Review of Microbiology* 63 (1): 195–221. doi:10.1146/annurev.micro.091208.073403.
23. Glick, D, A Barth, and K Macleod. 2010. “Autophagy: Cellular and Molecular Mechanisms.” *The Journal of Pathology* 221 (1): 3–12. doi:10.1002/path.2697.
24. Dupont, N, S Jiang, M Pilli, W Ornatowski, D Bhattacharya, and V Deretic. 2011. “Autophagy-Based Unconventional Secretory Pathway for Extracellular Delivery of IL-1β.” *The EMBO Journal* 30 (23): 4701–11. doi:10.1038/emboj.2011.398.
25. Kim, J, H Gee, and M Lee. 2018. “Unconventional Protein Secretion – New Insights into the Pathogenesis and Therapeutic Targets of Human Diseases.” *Journal of Cell Science* 131 (12). doi:10.1242/jcs.213686.
26. Navale, R, Atul, A Allanki, and P Sijwali. 2014. “Characterization of the Autophagy Marker Protein Atg8 Reveals Atypical Features of Autophagy in Plasmodium Falciparum.” *PLoS ONE* 9 (11). doi:10.1371/journal.pone.0113220.
27. Mehrpour, M, A Esclatine, I Beau, and P Codogno. 2010. “Overview of Macroautophagy Regulation in Mammalian Cells.” *Cell Research* 20 (7): 748–62. doi:10.1038/cr.2010.82.
28. Wesselborg, S, and B Stork. 2015. “Autophagy Signal Transduction by ATG Proteins: from Hierarchies to Networks.” *Cellular and Molecular Life Sciences* 72 (24): 4721–57. doi:10.1007/s00018-015-2034-8.
29. Cervantes, S, E Bunnik, A Saraf, C Conner, A Escalante, M Sardiu, N Ponts, J Prudhomme, L Florens, and K Roch. 2013. “The Multifunctional Autophagy

Pathway in the Human Malaria Parasite, Plasmodium Falciparum." *Autophagy* 10 (1): 80–92. doi:10.4161/auto.26743.

30. Totino, P Rivas, C Daniel-Ribeiro, S Corte-Real, and M Ferreira-Da-Cruz. 2008. "Plasmodium Falciparum: Erythrocytic Stages Die by Autophagic-like Cell Death under Drug Pressure." *Experimental Parasitology* 118 (4): 478–86. doi:10.1016/j.exppara.2007.10.017.
31. Short, B, A Haas, and F Barr. 2005. "Golgins and GTPases, Giving Identity and Structure to the Golgi Apparatus." *Biochimica Et Biophysica Acta* 1744 (3): 383–95. doi:10.1016/j.bbamcr.2005.02.001.
32. Rabouille, C, and A Linstedt. 2016. "GRASP: A Multitasking Tether. Frontiers in Cell and Developmental Biology." *Frontiers in Cell and Developmental Biology*, January. doi:10.3389/fcell.2016.00001.
33. Struck, N, S Herrmann, C Langer, A Krueger, B Foth, K Engelberg, A L. Cabrera, et al. 2008. "Plasmodium Falciparum Possesses Two GRASP Proteins That Are Differentially Targeted to the Golgi Complex via a Higher- and Lower-Eukaryote-like Mechanism." *Journal of Cell Science* 121 (13): 2123–29. doi:10.1242/jcs.021154.
34. Truschel, S, M Zhang, C Bachert, M Macbeth, and A Linstedt. 2012. "Allosteric Regulation of GRASP Protein-Dependent Golgi Membrane Tethering by Mitotic Phosphorylation." *Journal of Biological Chemistry* 287 (24): 19870–75. doi:10.1074/jbc.m111.326256.
35. Shorter, J, R Watson, ME Giannakou, M Clarke, G Warren, and FA Barr. 1999. "GRASP55, a Second Mammalian GRASP Protein Involved in the Stacking of

Golgi Cisternae in a Cell-Free System." *The EMBO Journal* 18 (18): 4949–60. doi:10.1093/emboj/18.18.4949.

36. Barr, FA, M Puype, J Vandekerckhove, and G Warren. 1997. "GRASP65, a Protein Involved in the Stacking of Golgi Cisternae." *Cell* 91 (2): 253–62. doi:10.1016/s0092-8674(00)80407-9.
37. Struck, N, S Herrmann, C Langer, A Krueger, B Foth, K Engelberg, A Cabrera, et al. 2008. "Plasmodium Falciparum Possesses Two GRASP Proteins That Are Differentially Targeted to the Golgi Complex via a Higher- and Lower-Eukaryote-like Mechanism." *Journal of Cell Science* 121 (13): 2123–29. doi:10.1242/jcs.021154.
38. Truschel, S T., D Sengupta, A Foote, A Heroux, M R. Macbeth, and A D. Linstedt. 2011. "Structure of the Membrane-Tethering GRASP Domain Reveals a Unique PDZ Ligand Interaction That Mediates Golgi Biogenesis." *Journal of Biological Chemistry* 286 (23): 20125–29. doi:10.1074/jbc.c111.245324.
39. Kinseth, M, C Anjard, D Fuller, G Guizzunti, W Loomis, and V Malhotra. 2007. "The Golgi-Associated Protein GRASP Is Required for Unconventional Protein Secretion during Development. ." *Cell*, July, 524–34. doi:10.1016/j.cell.2007.06.029.
40. Lingelbach, K, and K Joiner. 1998. "The Parasitophorous Vacuole Membrane Surrounding Plasmodium and Toxoplasma: an Unusual Compartment in Infected Cells." *Journal of Cell Science*, 1467–75.
41. Hallée, S, C Thériault, D Gagnon, J Kehrer, F Frischknecht, G R. Mair, and D Richard. 2018. "Identification of a Golgi Apparatus Protein Complex Important for

the Asexual Erythrocytic Cycle of the Malaria ParasitePlasmodium Falciparum." *Cellular Microbiology* 20 (8). doi:10.1111/cmi.12843.

42. Struck, N. S., S de Souza Dias, C Langer, M Marti, J Pearce, and A Cowman. 2005. "Re-Defining the Golgi Complex in Plasmodium Falciparum Using the Novel Golgi Marker PfGRASP." *Journal of Cell Science* 118 (23): 5603–13. doi:10.1242/jcs.02673.
43. Janse, C, J Ramesar, and A Waters. 2006. "High-Efficiency Transfection and Drug Selection of Genetically Transformed Blood Stages of the Rodent Malaria Parasite Plasmodium Berghei." *Nature Protocols* 1 (1): 346–56. doi:10.1038/nprot.2006.53.
44. Pichugin, A, and U Krzych. 2015. "Detection of Plasmodium Berghei and Plasmodium Yoelii Liver-Stage Parasite Burden by Quantitative Real-Time PCR." *Malaria Vaccines Methods in Molecular Biology*, 81–89. doi:10.1007/978-1-4939-2815-6_7.
45. Fölsch, H, M Pypaert, P Schu, and I Mellman. 2001. "Distribution and Function of Ap-1 Clathrin Adaptor Complexes in Polarized Epithelial Cells." *Journal of Cell Biology* 152 (3): 595–606. doi:10.1083/jcb.152.3.595.
46. Kaiser, K, N Camargo, and S Kappe. 2003. "Transformation of Sporozoites into Early Exoerythrocytic Malaria Parasites Does Not Require Host Cells." *Journal of Experimental Medicine* 197 (8): 1045–50. doi:10.1084/jem.20022100.
47. Sinnis, P, and A Coppi. 2007. "A Long and Winding Road: The Plasmodium Sporozoites Journey in the Mammalian Host." *Parasitology International* 56 (3): 171–78. doi:10.1016/j.parint.2007.04.002.

48. Shears, M, R Sekhar Nirujogi, K Swearingen, S Renuse, S Mishra, P Jaipal Reddy, R Moritz, A Pandey, and P Sinnis. 2019. “Proteomic Analysis of Plasmodium Merosomes: The Link between Liver and Blood Stages in Malaria.” *Journal of Proteome Research* 18 (9): 3404–18. doi:10.1021/acs.jproteome.9b00324.s001.
49. Hain, A, and J Bosch. 2013. “Autophagy in Plasmodium, a Multifunctional Pathway?” *Computational and Structural Biotechnology*. Accessed August 20. doi:10.5936/csbj.201308002.
50. Zhang, X, and Y Wang. 2016. “GRASPs in Golgi Structure and Function.” *Frontiers in Cell and Developmental Biology* 3 (June). doi:10.3389/fcell.2015.00084.

Curriculum Vitae

Ella Gehrke

EDUCATION

May 2020	**Master of Science (ScM)** Molecular Microbiology & Immunology Johns Hopkins Bloomberg School of Public Health (JHSPH), *Baltimore, MD*
May 2020	**Certificate in Tropical Medicine** JHSPH Department of Molecular Microbiology & Immunology, *Baltimore, MD*
December 2017	**Bachelor of Science (BS) Global Resource Systems** Iowa State University, *Ames, IA* **Minors:** Biology, Emerging Global Diseases

PROFESSIONAL EXPERIENCE

2019-2020	**Graduate Teaching Assistant,** Johns Hopkins University Bloomberg School of Public Health
2018-2020	**Graduate Research Assistant**, Johns Hopkins University Bloomberg School of Public Health - Coppens Lab (*Baltimore, MD)*
2016-2018	**Research Assistant**, Iowa State University Medical Entomology Laboratory (*Ames, IA)*
2018	**Live Out Assistant**, Friendship Ark Homes (*Ames, IA)*
2017	**Research Fellow**, Midwest Center of Excellence for Vector-Borne Disease (*Ames, IA)*
Summer 2016	**Center for Sustainable Rural Livelihoods Intern** (*Kamuli District, Uganda)*
2014-present	**Co-founder**, KinoSol SBC. *(Ames, IA)*
2014, 2015	**George Washington Carver Intern***,* World Food Prize *(Des Moines, Iowa)*

VOLUNTEER EXPERIENCE

2018-present	**HIV Testing Counselor**, The Johns Hopkins Hospital Emergency Department, *(Baltimore, MD)*
2015-2018	**Mae E. Davis Free Medical Clinic Administrator**, (*West Des Moines, Iowa)*

PUBLICATIONS

October 2019	Field, E. N., Gehrke, E. J., Smith, R. C. (in review). An improved multiplex PCR assay for the identification of mosquito (Diptera: Culicidae) blood meals. *Journal of Medical Entomology.*
April 2019	Dunphy, B. M., Kovach, K. B., Gehrke, E. J., Field, E. N., Rowley, W. A., Bartholomay, L. C., & Smith, R. C. (2019). Long-term surveillance defines spatial and temporal patterns implicating *Culex tarsalis* as the primary vector of West Nile virus in Iowa, USA. *Cold Spring Harbor Laboratory*. doi: https://doi.org/10.1101/476234